Molecular Therapy
Original Article

Synergic activity of FGFR2 and MEK inhibitors in the treatment of FGFR2-amplified cancers of unknown primary

Andrea Cavazzoni,[1,12] Irene Salamon,[2,12] Claudia Fumarola,[1,12] Giulia Gallerani,[3] Noemi Laprovitera,[2] Francesco Gelsomino,[2] Mattia Riefolo,[2,3] Karim Rihawi,[2] Elisa Porcellini,[3] Tania Rossi,[4] Martina Mazzeschi,[3] Maria Naddeo,[2] Salvatore Serravalle,[2] Elisabetta Broseghini,[2] Federico Agostinis,[5,10] Olivier Deas,[6] Roberta Roncarati,[3,7] Giorgio Durante,[3] Ilaria Pace,[3] Mattia Lauriola,[3] Ingrid Garajova,[8] George A. Calin,[9] Massimiliano Bonafè,[2,3] Antonia D'Errico,[2,3] Pier Giorgio Petronini,[1] Stefano Cairo,[6,11] Andrea Ardizzoni,[2,3] Gabriele Sales,[5,13] and Manuela Ferracin[2,3,13]

[1]Department of Medicine and Surgery, University of Parma, 43126 Parma, Italy; [2]IRCCS, Azienda Ospedaliero-Universitaria di Bologna, 40126 Bologna, Italy; [3]Department of Medical and Surgical Sciences (DIMEC), University of Bologna, 40126 Bologna, Italy; [4]Biosciences Laboratory, IRCCS Istituto Romagnolo per lo Studio dei Tumori (IRST) "Dino Amadori", Meldola 47014, Italy; [5]Department of Biology, University of Padova, 35031 Padua, Italy; [6]XenTech, Evry 91100, France; [7]Istituto di Genetica Molecolare "Luigi Luca Cavalli-Sforza" (IGM)- Consiglio Nazionale delle Ricerche (CNR), 40136 Bologna, Italy; [8]Medical Oncology Unit, University Hospital of Parma, 43126 Parma, Italy; [9]Department of Experimental Therapeutics, The University of Texas MD Anderson Cancer Center, Houston, TX 77030, USA

Patients with cancer of unknown primary (CUP) carry the double burden of an aggressive disease and reduced access to therapies. Experimental models are pivotal for CUP biology investigation and drug testing. We derived two CUP cell lines (CUP#55 and #96) and corresponding patient-derived xenografts (PDXs), from ascites tumor cells. CUP cell lines and PDXs underwent histological, immune-phenotypical, molecular, and genomic characterization confirming the features of the original tumor. The tissue-of-origin prediction was obtained from the tumor microRNA expression profile and confirmed by single-cell transcriptomics. Genomic testing and fluorescence *in situ* hybridization analysis identified *FGFR2* gene amplification in both models, in the form of homogeneously staining region (HSR) in CUP#55 and double minutes in CUP#96. FGFR2 was recognized as the main oncogenic driver and therapeutic target. FGFR2-targeting drug BGJ398 (infigratinib) in combination with the MEK inhibitor trametinib proved to be synergic and exceptionally active, both *in vitro* and *in vivo*. The effects of the combined treatment by single-cell gene expression analysis revealed a remarkable plasticity of tumor cells and the greater sensitivity of cells with epithelial phenotype. This study brings personalized therapy closer to CUP patients and provides the rationale for FGFR2 and MEK targeting in metastatic tumors with FGFR2 pathway activation.

INTRODUCTION

Metastases develop when tumor cells spread from the primary site to surrounding or distant tissues and are responsible for 90% of cancer-related deaths.[1] Among metastatic patients, 3%–5% show no clinical evidence of a primary site at diagnosis. These cases are classified as cancers of uncertain origin or cancers of unknown primary site (CUPs) or occult primary tumors.[2,3] They are usually diagnosed at a late stage, with patients presenting one or more metastases already at the first diagnosis. The identification of the tumor primary site is usually obtained by a combination of diagnostic investigations including physical examinations, blood analyses, imaging, and immunohistochemical (IHC) testing of the tumor tissue. In CUP patients, these investigations are inconclusive.

International guidelines for tumor treatment are based on primary site indication. Therefore, CUP treatment requires a blind approach, which is very challenging for oncologists. Consequently, CUPs are typically treated with empiric platinum-based chemotherapy regimens, which are usually poorly effective. Indeed, CUP patients have a short life expectancy (average overall survival 4–9 months, with only 20% surviving more than 1 year), which, unfortunately, did not improve over the last decades. However, these regimens remain empirical since they are mostly based on results of single-arm phase II clinical trials[4–6] or small phase III trials.[7–9]

Received 5 November 2023; accepted 17 July 2024;
https://doi.org/10.1016/j.ymthe.2024.07.011.

[10]Present address: Associate Data Analyst & Data Scientist at Evotec SE, Hamburg, Germany

[11]Present address: Senior global scientific director at Champions Oncology, USA

[12]These authors contributed equally

[13]These authors contributed equally

Correspondence: Manuela Ferracin, IRCCS, Azienda Ospedaliero-Universitaria di Bologna, 40126 Bologna, Italy.
E-mail: manuela.ferracin@unibo.it

Please cite this article in press as: Cavazzoni et al., Synergic activity of FGFR2 and MEK inhibitors in the treatment of FGFR2-amplified cancers of unknown primary, Molecular Therapy (2024), https://doi.org/10.1016/j.ymthe.2024.07.011

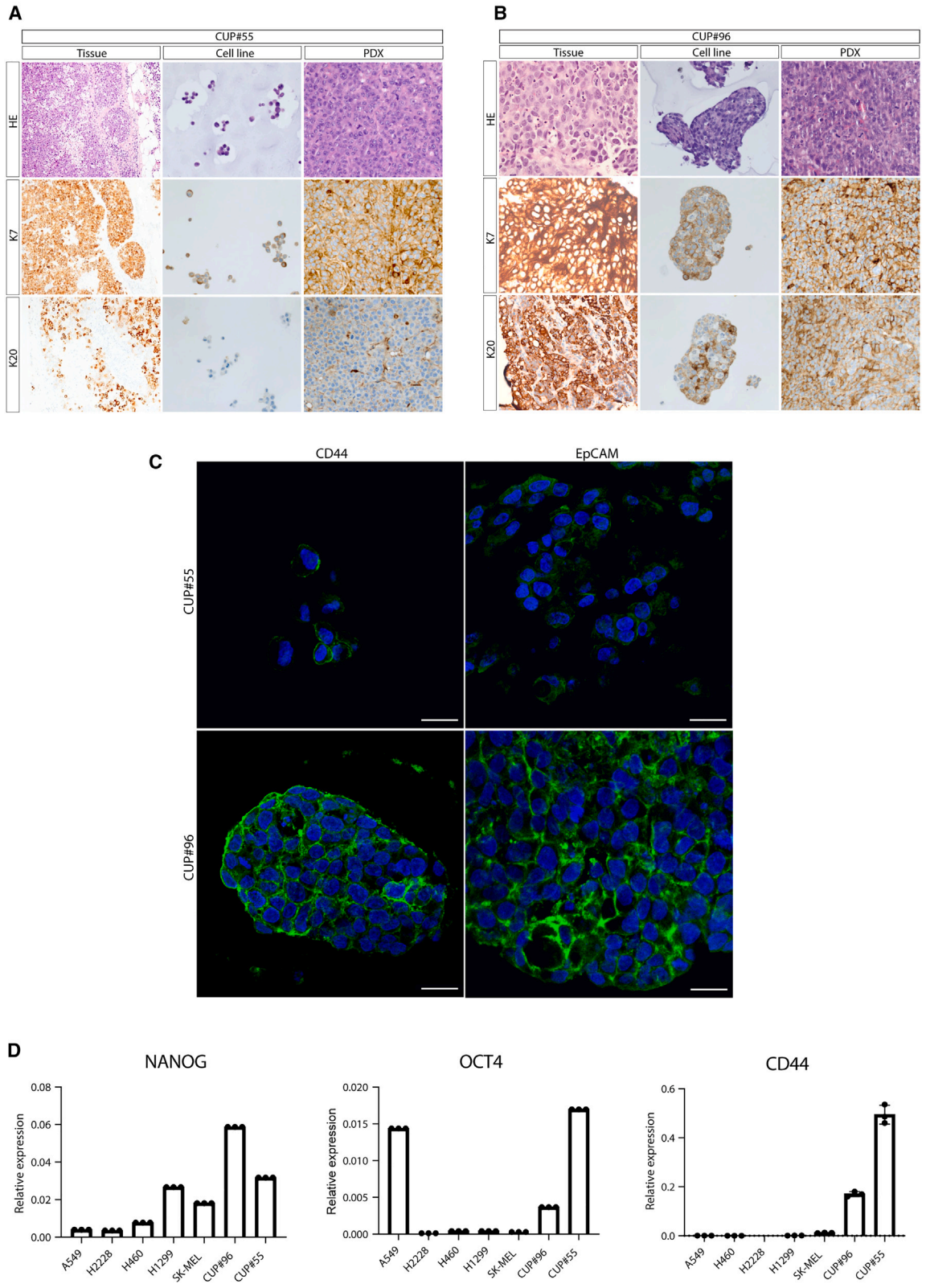

(legend on next page)

Please cite this article in press as: Cavazzoni et al., Synergic activity of FGFR2 and MEK inhibitors in the treatment of FGFR2-amplified cancers of unknown primary, Molecular Therapy (2024), https://doi.org/10.1016/j.ymthe.2024.07.011

The use of molecular tests based on gene or microRNA (miRNA) expression signatures or methylation profiles to identify the most probable site of origin could assist the oncologists in the selection of the best treatment options and potentially improve CUPs outcome.[3,10]

With the advent of personalized medicine, patient management is more and more frequently associated with the identification of specific molecular or genetic features of the tumor upon which therapies could be based to avoid suboptimal treatments. The identification of druggable alterations in CUP tumors could increase the otherwise limited treatment options, as recently demonstrated by Hayashi et al.[11] Next generation sequencing technologies were applied to the analysis of CUP mutational profile.[12–16] Overall, CUPs seem to harbor recognized actionable genetic alterations in nearly 30% of cases.[3,17] Immunotherapy has been scarcely tested on CUP patients: in a study by Gatalica et al. only a fraction of patients presented favorable biomarkers for the use of immune checkpoint inhibitors[18] but among those who have high tumor mutational burden (TMB), the use of immunotherapy extends survival. Varghese and Saltz identified the actionable mutations in a dataset of 150 CUPs analyzed with the MSK-IMPACT panel reporting that patients who were eligible for targeted therapies, showed clinical benefit and longer survival.[14] A meta-analysis conducted by Ding et al. confirmed a benefit for site-specific therapies only for CUP patients with a strong primary site prediction score.[19]

However, even today the knowledge that molecular and genetic testing could provide novel personalized treatments for CUP patients is hampered by the lack of cellular and animal models on which to test potentially effective therapies.

A main limitation in the development of CUP models is posed by the reduced availability of fresh tumor cells, given that the biopsy is frequently entirely dedicated to the diagnostic workup and surgery is rarely an option for these patients. Circulating tumor cells have been tracked in the blood of CUP patients[20,21] and could be the source of tumor cells for cell line/patient-derived xenograft (PDX) development; this is true also for ascitic fluid, which can become a valuable source of viable tumor cells. In addition to being more accessible, liquid biopsy tumor cells would have the advantage of being more representative of the overall complexity and heterogeneity of CUP tumors.

In this study, we obtained and expanded two patient-derived CUP cell lines from ascites tumor cells, spontaneously growing as spheroids and organoids, and corresponding PDXs. We obtained the immunophenotypic, molecular, and genomic characterization of the tumor and derived models, confirming the recapitulation of the original features. MicroRNA profiling was used to predict the possible primary site. We identified FGFR2 as a driver actionable gene in both our CUP models and tested a combination of drugs with promising antitumor activity, both *in vitro* and *in vivo*. Single-cell resolved transcriptomic analysis was used to monitor CUP plasticity during treatment.

RESULTS

Establishment of two CUP models from ascites tumor cells: Immunophenotypical, genetic, and molecular characterization

We generated *in vitro* and *in vivo* CUP models to test tailored experimental pharmacological approaches. CUP patient #55 was diagnosed with multiple lymph node metastases of poorly differentiated adenocarcinoma. Immunohistochemistry (IHC) staining reported the positivity for keratin 7 (KRT7) and CDX2, weak positivity for keratin 20 (KRT20), and negativity for neuroendocrine markers (chromogranin, synaptophysin, NCAM1). CUP patient #96 presented with multiple metastases of poorly differentiated adenocarcinoma with peritoneal carcinosis and multiple sub- and supra-diaphragmatic lymph node metastases. The tumor IHC staining was positive for KRT7, KRT20, CDX2, and EPCAM and negative for PAX8, P40, GATA3, and calretinin.

Two long-term (more than 10 passages[22]) cell lines (CUP#55 and CUP#96) were obtained isolating cells from ascites fluid of the patients #55 and #96, respectively. One month after seeding, cells growing in suspension were visible as spheroid-like structures (Figure S1). The growth curve of two models was monitored for 10 days using the Incucyte S3 live-cell analysis: 10,000 cells were seeded and after few hours CUP#96 cells formed large tumoroids and CUP#55 cells organized as clusters, showing a doubling time of 5 days for both cell lines (Figures S2 and S3).

We generated two PDX models by injecting ascites tumor cells in the interscapular region of immunocompromised mice. The two models showed different growth rate, with CUP#96 PDX growing faster than CUP#55 PDX, and with CUP#55 PDX inducing a tumor-intrinsic mild cachexia in the mice (Figure S4). Morphology and histology of the cell lines and PDXs recapitulated the features of their respective primary tumors (Figures 1A and 1B), thus confirming the reliability of the models.

Among the hypotheses on CUP origin, there is the rapid acquisition of an EMT-driven metastatic phenotype from a few primary tumor

Figure 1. Immunophenotypic characterization of CUP samples

(A) Immunophenotypic characterization of tumor tissue, cell line, and PDX of CUP#55. Hematoxylin-eosin (HE), keratin7 (KRT7), and keratin20 (KRT20) IHC staining of CUP#55 tumor tissue, cell line, and PDX (40×). The staining showed that the cell line and PDX tumor recapitulate the histology of the patient's tumor tissue. (B) Immunophenotypic characterization of tumor tissue, cell line, and PDX of CUP#96. HE, KRT7, and KRT20 IHC staining of CUP#96 tumor tissue, cell line, and PDX (40x). CUP#96 cell line grows forming tumoroid structures. The staining showed that the cell line and PDX tumor recapitulate the histology of the patient's tumor tissue. (C) Immunophenotypic analysis of CUP #55 and #96 cell lines demonstrating the expression of cancer stem cell markers CD44 and EPCAM. Staining: nucleus (DAPI, blue), CD44 and EPCAM (green). Scale bars, 20 μm. (D) Gene expression analysis of stemness genes in CUP#55 and CUP#96. Bars represent the relative expression of genes using HPRT as reference gene and the $2^{-\Delta Ct}$ method. The expression in CUP cell lines was compared with other cancer cell lines from lung and melanoma origin.

cells or the malignant transformation of tissue stem cells. To verify whether CUP tumor cells presented a stem cell-like phenotype, the two tumoroid cell lines were tested for CD44 and EPCAM immunoreactivity and the gene expression of stemness genes CD44, NANOG, and POU5F1 (Figures 1C and 1D). The two cell lines express CD44 on their surface, which is more homogeneous for CUP#96 (Figure 1C), and both express stemness genes at high levels if compared with a panel of cancer cell lines (Figure 1D).

We recently developed a predictive microRNA-based test to assign a possible primary site to metastatic cancers, including occult primary tumors.[3,23] We applied our on-demand, droplet digital PCR-based, multi-miRNA assay and cancer-type classifier for the prediction of CUP primary tumor site to the two cell lines and obtained a site-of-origin prediction: CUP#55 was predicted to be of biliary tract origin (with a probability of 93%) and CUP#96 of gastrointestinal tract origin (with a probability of 99%). The absolute miRNA expression of the 92 miRNAs of the predictive panel in CUP#55 and 96 cell line, CUP#PDX and formalin-fixed paraffin-embedded (FFPE) is available as Table S1.

We characterized the main genetic alterations of CUP#55 and CUP#96 tumors, in patients' and models' samples. From the patients we collected and analyzed the tumor tissue and circulating cell-free DNA (ccfDNA). DNA was also collected from the two cell lines and PDXs. All samples were tested for genetic alterations with a CUP-dedicated, 92-gene custom panel we previously described,[20] using SureSelect Target Enrichment technology (Agilent Technologies). The genes were selected as the most frequently altered genes in CUPs, as reported in the MSK Impact study[15] and AACR Genie project[24] CUP cohorts, including druggable or potentially actionable alterations. The summary of all genetic alterations is reported in Tables 1 and 2. The genetic analysis of CUP#55 identified five genetic alterations shared by all the analyzed samples (bulk tumor DNA, ccfDNA, cell line, and PDX): the base insertion in the *APC* gene (p.T1556fs*3) and the point mutations in *ARID1A* (p.R1276*), *ERBB3* (p.S128R), *KEAP1* (p.R135H), and *NTRK1* (p.Q736X). Mutations in *ALK, EPHA5, FAT1, KMT2C, MGA, PTPRD* (except for p.L970V), and *TP53* were detected only in ccfDNA (Table 1). As expected, the variant allele fractions (VAFs) were higher in PDX and cell line, thus reflecting the enrichment in tumor cells and the possible selection of tumor subclones, if compared with the tumor biopsy. Low-frequency mutations in *ZFHX3, RBM10, PTPRT, NF1, MED12, MGA, KDR, KDM5A, GRIN2A, EP300, DOT1L,* and *APC* (p. S887R) were identified in the models but not in other samples.

The genetic analysis of CUP#96 was conducted on ccfDNA and cell line DNA due to the unavailability of the residual tumor FFPE sample for this patient, a condition that frequently occurs for CUP samples. Five genetic alterations were detected both in ccfDNA and cell line (Table 2), with higher VAFs in the cell line compared with ccfDNA.

We analyzed the gene amplification (copy number gain) and deletion (copy number loss) using Shallow Sequencing (Low-Pass) Copy Number Analysis on the two cell lines. We identified several regions of amplification and deletion (Tables S2 and S3), including a >10 copies amplification in chromosome 10 encompassing *FGFR2* oncogene in both cell lines. Interestingly, CUP#55 is characterized by *MET*, *MYC,* and *CCNE1* amplification; CUP#96 has *APC* and *CDKN2A* deletion and *MET* and *MYC* amplification.

CUP#55 characterization using single-cell transcriptomics

We characterized the CUP#55 cell line with a single-cell (sc) transcriptomic approach based on 10X Single-Cell 5′ R2-only kit. After filtering for low-quality droplets and potentially dying cells (high expression of mitochondrial genes), we obtained the sc transcriptome of about 1,500 cells. Automated cell type annotation using the scType method identified liver as the most similar tissue for this cell line (Figure 2A). It is relevant to notice that while bile duct was not directly included in the catalog of tissues whose marker genes are evaluated by the software, this approach was the best option we had to "confirm" the prediction based on miRNA profiles. The CUP#55 cell line morphology is uniform in cell culture, but when cells were clustered based on their reciprocal similarity, the scType algorithm led to the identification of two separate clusters (Figure 2B), labeled cluster 1 and cluster 2, with significant differences in their expression profiles. We identified two sets of positive marker genes that characterize each cluster. Specifically, we obtained a total of 1,051 markers for cluster 1 and 3,059 for cluster 2 (Table S4). Functional annotation with MetaCore of the markers for cluster 1 highlighted an over-representation for pathways including antigen presentation, cytoskeleton remodeling, and cell adhesion (Figure S5). A similar analysis of cluster 2 markers identified the following enriched pathways: regulation of Wnt/beta-catenin pathway, VEGFR2 signaling, and Double-strand break repair.

The single-cell gene expression analysis confirmed the abundant expression of *FGFR2* and *EPCAM* and the variable expression of gene markers of EMT and stemness (Figure 2C), with *SNAI1* and *TGFB1* more expressed in cells belonging to cluster 1, and *CD44*, *ZEB1*, and *HIF1A* in cells of cluster 2.

We then applied a mapping approach (Azimuth) using an atlas of liver cells as a reference, with the objective of inferring the most likely type of origin for CUP cells in each cluster. While 93% of cells in cluster 1 were annotated as cholangiocytes (Figure S6A), the classification of cluster 2 was more diverse: specifically, mapped types were split between cholangiocytes (73% of cells) and T/NK cells (27%). As this separation did not correspond to any difference in cell morphology, we double-checked the association manually. We identified the marker genes for the T/NK subgroup (Table S5) and noticed that most of the genes are implicated in the cell cycle, and in particular with the mitotic phase and DNA repair, as demonstrated by the results of MetaCore pathway enrichment analysis (Figure S6B). Moreover, the list lacks the main markers that characterize the T/NK group in Azimuth liver atlas (*CCL5*, *KLRB1*, *NKG7*, *CD69*, *GZMA*, *CCL4*, *CST7*, *GNLY*, *GZMK*) and none of the cells in cluster 2 expresses any of those genes. This suggests that the identification of T/NK cells

Table 1. Genetic alterations detected in CUP#55 patient-derived tissues and models

Gene	Coding change	Aminoacidic change	Tumor FFPE	ccfDNA at diagnosis	ccfDNA at disease progression	Cell line	PDX passage 1	Predicted as pathogenic[a]
ALK	c.A1301G	p.K434R	not detected	not detected	7.0%	not detected	not detected	no
APC	4607insA	p.T1556fs3[a]	9.8%	22.6%	29.9%	100.0%	95.0%	ND
APC	c.A2659C	p.S887R	not detected	not detected	not detected	43.2%	not detected	yes
ARID1A	c.C3826T	p.R1276X	8.9%	28.5%	22.8%	53.0%	19.8%	yes
CREBBP	c.T1448C	p.L483P	not detected	not detected	not detected	not detected	21.7%	ND
DOT1L	c.A1193C	p.K398T	not detected	not detected	not detected	38.2%	not detected	yes
EP300	c.A7118C	p.N2373T	not detected	not detected	not detected	not detected	32.2%	no
EPHA5	c.A1417C	p.T473P	not detected	not detected	8.3%	not detected	not detected	no
ERBB3	c.C384A	p.S128R	9.8%	20.7%	20.4%	41.09%	48.60%	yes
ERBB4	c.T343A	p.Y115N	not detected	not detected	not detected	not detected	33.8%	yes
FAT1	c.A2084C	p.N695T	not detected	not detected	2.6%	not detected	not detected	no
GRIN2A	c.A4064C	p.K1355T	not detected	not detected	not detected	not detected	22.3%	no
KDM5A	c.T3547C	p.W1183R	not detected	not detected	not detected	not detected	22.2%	yes
KDR	c.A981C	p.K327N	not detected	not detected	not detected	not detected	27.9%	ND
KEAP1	c.G404A	p.R135H	9.0%	22.6%	19.5%	51.8%	44.0%	yes
KMT2C	c.C2459T	p.T820I	not detected	1.1%	1.1%	not detected	not detected	yes
KMT2C	c.C1013T	p.S338L	not detected	5.5%	4.3%	not detected	not detected	no
KMT2C	c.C2689T	p.R897X	not detected	not detected	1.4%	not detected	not detected	yes
KMT2C	c.C2228T	p.P743L	not detected	not detected	1.6%	not detected	not detected	no
MED12	c.A688C	p.I230L	not detected	not detected	not detected	not detected	25.0%	no
MGA	c.A395C	p.N132T	not detected	not detected	not detected	not detected	30.5%	yes
MGA	c.T4004C	p.L1335P	not detected	not detected	1.6%	not detected	not detected	ND
NF1	c.A6083G	p.K2028R	not detected	not detected	not detected	not detected	25.4%	yes
NTRK1	c.C2206T	p.Q736X	8.3%	26.0%	22.3%	32.6%	44.7%	yes
PALB2	C2419T	p.P807S	9.0%	19.1%	16.6%	not detected	47.4%	no
PTPRD	c.T2908G	p.L970V	not detected	5.1%	3.5%	not detected	47.7%	yes
PTPRD	c.A3117C	p.Q1039H	not detected	not detected	6.8%	not detected	not detected	yes
PTPRT	c.T479C	p.F160S	not detected	not detected	not detected	not detected	33.8%	no
RBM10	c.A2024G	p.K675R	not detected	not detected	not detected	not detected	41.7%	no
TP53	c.C9G	p.C3W	not detected	1.2%	not detected	not detected	not detected	yes
TP53	c.A355G	p.I119V	not detected	1.7%	not detected	not detected	not detected	yes
TP53	c.G315C	p.M105I	not detected	1.8%	not detected	not detected	not detected	yes
TP53	c.T316C	p.C106R	not detected	2.1%	not detected	not detected	not detected	yes
ZFHX3	c.A1604C	p.E535A	not detected	not detected	not detected	not detected	27.5%	no
ZFHX3	c.A7529G	p.Q2510R	not detected	not detected	not detected	not detected	39.7%	no

[a]Variants were considered pathogenic when more than 50% of the eight predictors (SIFT, Polyphen2 HVAR, LRT, Mutation Taster, Mutation Assessor, FATHMM, CADD and VEST) considered the alteration as pathogenic/damaging/deleterious/harmful. ND, not defined.

by reference mapping is likely incorrect and driven by the confounding effect of the cell cycle (Figure S6C).

We concluded that all the cells in the CUP#55 model belong all to the same cell type (liver/cholangiocytes) but they show a degree of plasticity that results in two closely related, but distinct states, represented by the two clusters.

FGFR2 amplification in CUP#55 and CUP#96 cell lines provides the rationale to target the receptor using a selective inhibitor

FGFR2 genomic alterations are detected in CUPs with a frequency ranging from 3% to 4% according to AACR GENIE and MSK-IMPACT studies (Figure S7). Our patient-derived CUP models are both characterized by *FGFR2* amplification, which we confirmed using the Fluorescence *In Situ* Hybridization (FISH) technique and droplet

Table 2. Genetic alterations detected in CUP#96 patient-derived tissues and models

Gene	Coding change	Aminoacidic change	CUP#96 cell line	ccfDNA at diagnosis	Predicted as pathogenic[a]
PIK3C2G	c.G1813A	p.V605I	100.00%	48.35%	no
TP53	c.G418A	p.V140M	100.00%	49.34%	yes
SMAD4	c.A1610G	p.D537G	100.00%	44.23%	yes
KMT2C	c.G943A	p.G315S	4.58%	5.31%	yes
CTNNB1	c.C110T	p.S37F	55.10%	22.39%	yes
KMT2C	c.A2725G	p.R909G	–	6.48%	yes
KMT2C	c.C3274T	p.R1092X	–	5.28%	yes
KMT2C	c.C1013T	p.S338L	–	4.57%	no
KMT2C	c.G944A	p.G315D	–	3.09%	yes

[a]Variants were considered pathogenic when more than 50% of the eight predictors (SIFT, Polyphen2 HVAR, LRT, Mutation Taster, Mutation Assessor, FATHMM, CADD and VEST) considered the alteration as pathogenic/damaging/deleterious/harmful. ND, not defined.

digital PCR (ddPCR) for absolute copy number quantification. FISH demonstrated the different nature of *FGFR2* amplification: CUP#96 displays an extrachromosomal DNA amplification in the form of double minutes; CUP#55 shows a homogeneously staining region (HSR) associated with *FGFR2* chromosomal amplification (Figure 3A). The copy number variation (CNV) of the *FGFR2* gene was confirmed by ddPCR using a probe-based assay in the circulating cell-free (ccfDNA), cell line and PDX of both patients (Figure 3B). *FGFR2* copy number (CN) in tumor DNA was >60 for CUP#55 and >400 for CUP#96 across all samples. Consistent with the CN amplification, *FGFR2* gene expression is significantly increased in both cell lines (Figure 3C) compared with other tumor cell lines (p value <0.001).

FGFR2 locus encode for 10 FGFR2 isoforms, with *FGFR2IIIb* and *FGFR2IIIc* as the main transcripts. In particular, the *FGFR2IIIb* isoform is expressed mainly in epithelial cells, and the *FGFR2IIIc* isoform is preferentially expressed in mesenchymal cells.[25,26] As a potential indicator of epithelial-mesenchymal transition, we monitored the expression of the two FGFR2 isoforms in the cell lines and found that they express the epithelial *FGFR2IIIb* isoform at high levels but also the mesenchymal *FGFR2IIIc* isoform (Figure S8).

Western blot analysis confirmed that CUP#96 cells express higher levels of total FGFR2 protein compared with CUP#55 cells. Interestingly, in both models, the FGFR2 appears constitutively phosphorylated (Figure 3D). Notably, the FGFR2 phosphorylation/expression is higher than in a reference FGFR2-positive cell line (H1581), derived from a lung adenocarcinoma with FGFR1 and FGFR2 amplification[27] (Figures 3C and 3D). FGFR2 gene amplification and activation in CUP#55 and CUP#96 cells provided the rationale for the pharmacological targeting of this receptor for therapeutic intervention.

Simultaneous inhibition of FGFR2/AKT and MAPK pathways by BGJ398 and trametinib, respectively, induces synergistic antiproliferative and pro-apoptotic effects in CUP models *in vitro*

We preliminarily tested a panel of multikinase inhibitors (BGJ398, dovitinib, ponatinib) for their effect on CUP#55 cell vitality. We selected BGJ398 (infigratinib), a selective inhibitor of the FGFR family, for its greater effect on cell viability (Figure S9) for further testing in CUP#55 and CUP#96 cells. In CUP#55, the treatment with this drug at different concentrations (range 0.5–2.5 μM) inhibited FGFR2 phosphorylation and the downstream AKT/MTOR/p70S6K signaling (Figure 4A). In contrast, ERK1/2 remained phosphorylated even at the highest BGJ398 concentration. CUP#55 cells were sensitive to BGJ398 treatment, although a complete inhibition of their viability/proliferation was not achieved even at 1μM BGJ398 concentration, suggesting that FGFR-independent mechanisms sustain the activation of the MAPK pathway and contribute to cell growth in this model. These results prompted us to test whether targeting the MAPK pathway with trametinib, a highly specific inhibitor of MAP2K1/2 proteins, might improve the efficacy of BGJ398 treatment. The drug combination inhibited both the AKT and MAPK pathways almost completely (Figure 4B), thereby evidencing a highly significant synergistic inhibition of cell proliferation, as indicated by the comparison with the theoretical interaction curve in the Bliss experimental model ($p < 0.001$) (Figure 4C). Interestingly, even if the single treatment with either BGJ398 or trametinib did not induce cell death in CUP#55 cells, their combination had a cytotoxic effect, as demonstrated by fluorescence microscopy analysis of Hoechst 33342/PI-stained cells; the morphology of the stained nuclei suggested that the cells died by apoptosis (Figure S10A), a result confirmed by Annexin V-FITC/PI staining (Figure S10B) and caspase-3 cleavage (Figure 4E).

Then, we analyzed the effects of FGFR2 inhibition by BGJ398 treatment in CUP#96 cells. Inhibition of FGFR2 phosphorylation by BGJ398 treatment resulted in the downregulation of phosphorylated forms of AKT, p70S6K, and ERK1/2 levels, suggesting that both AKT and MAPK pathways are downstream of FGFR2 in this cell model (Figure 5A). We tested the combination of BGJ398 with trametinib also in these cells and found that it produced a remarkable synergistic inhibition of MAPK signaling and cell proliferation (Figures 5B and 5C), comparable to that observed in CUP#55 cells, suggesting that trametinib can provide a more effective inhibition of the MAPK

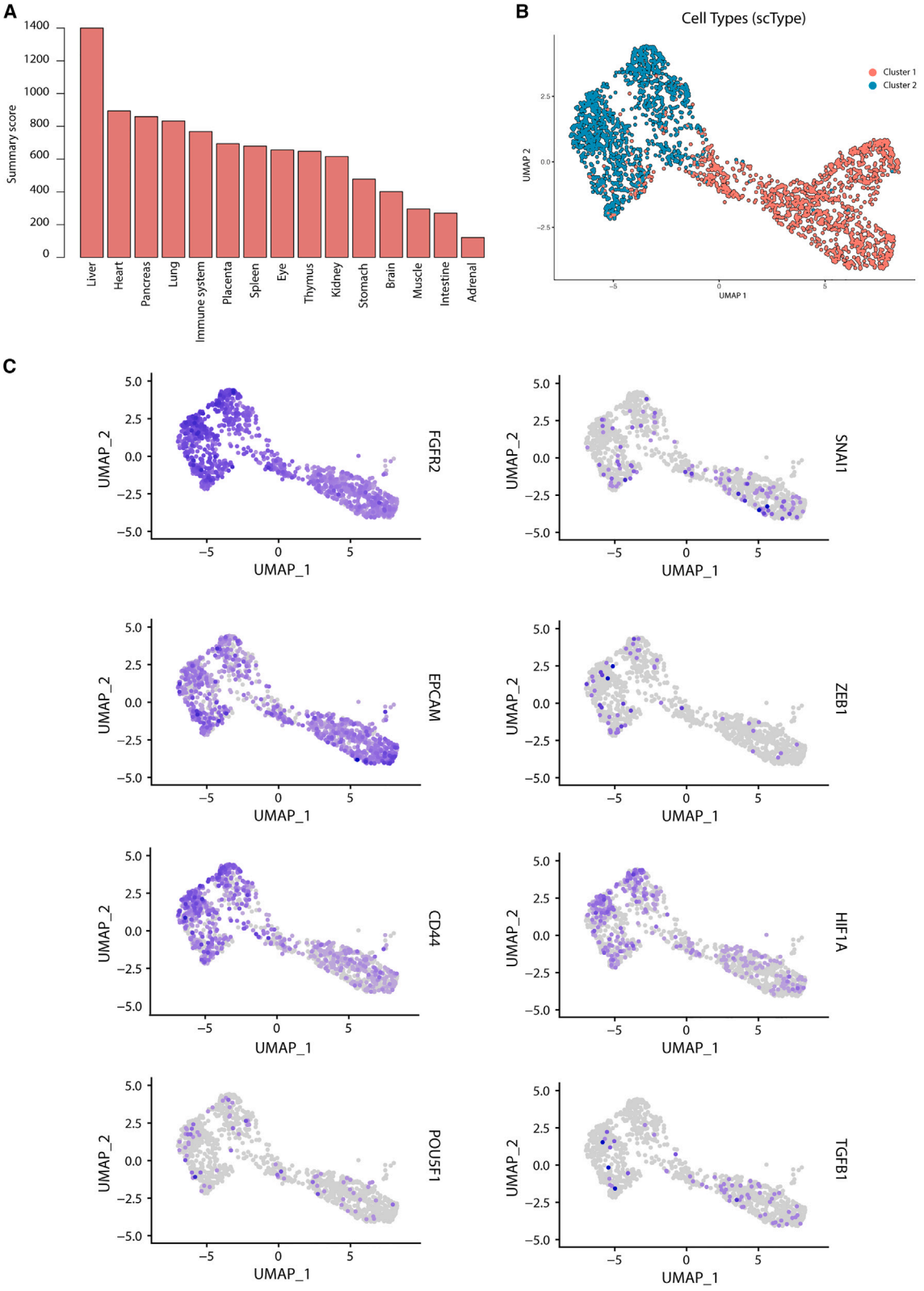

(legend on next page)

pathway leading to suppression of cell growth also in this cell model. Of note, BGJ398 and trametinib alone were cytotoxic in CUP#96 cells, an effect that was further enhanced by the combined treatment (Figure 5D). Caspase-3 cleavage confirmed the induction of cell death by apoptosis also in this model (Figure 5E) by the combined treatment. Altogether, these findings indicate that trametinib significantly improves the antitumor effect of FGFR2 targeting in FGFR2-amplified CUP cells.

In vivo synergic activity of FGFR2 and MEK inhibitors

We tested whether *in vitro* findings on FGFR2 and MEK inhibitors synergic activity could be recapitulated in CUP#55 and CUP#96 PDX models *in vivo*.

Mice were treated with control vehicle, BGJ398 (15 mg/kg), trametinib (0.6 mg/kg), and trametinib/BGJ398 combination (n = 5 per group) for up to 14 days. The scheme of the different treatments is reported in Figures 6A and 6B; the effect of different drugs was evaluated measuring the tumor volume. Single drug BGJ398 or trametinib treatment significantly reduced the tumor volume in PDX#96 xenograft mice if compared with tumors of mice treated with vehicle but only BGJ398 significantly reduced the tumor volume in PDX#55 xenografts mice (p value < 0.05). However, the combination of trametinib and BGJ398 was more effective than the single treatments in both PDX models, as demonstrated by the dramatic reduction of the tumor volume (Figures 6A and 6B) as evidenced by two-way ANOVA statistical test (p value < 0.0001). CUP#55 PDX mice suffered from tumor-induced cachexia and for this reason they were euthanized after 2 weeks of treatment. CUP#96 PDX mice treated with the combination were still alive at 6 weeks.

Transcriptome shift induced by treatment

We analyzed the early effects of the combined treatment with MEK and FGFR2 inhibitors on CUP#55 transcriptome at the sc level. The treatment affected the transcriptional activity of the cells in the two main clusters, with a stronger effect on cells of cluster 2: we identified 854 and 4,787 differentially expressed genes (DEGs) between the treated (T) and untreated (C) cells, respectively, in clusters 1 and 2, and 1,204 DEGs considering all cells (Table S6). A guided gene set enrichment analysis confirmed that the epithelial-mesenchymal transition was influenced by the treatment, although at different degrees in the two clusters. Specifically, the signature identified by Tuan et al.[28] was the most enriched in cluster 1 (NES −2.36, adjusted p value $7.81E^{-4}$), while the signature from Cursons et al.[29] was the most significant in cluster 2 (NES -3.09, adjusted p value $3.56E^{-8}$). The negative sign in both enrichment scores corresponds to an overall downregulation of genes promoting the epithelial phenotype, suggesting a greater impact of the treatment on cells with an epithelial phenotype.

With the aim of understanding the effects of the combined treatment on CUP cells, we performed a pathway enrichment analysis on the three lists of DEGs (all cells, cluster 1, cluster 2) (Table S7). Overall, the most affected functions were VEGFR and EGFR signaling, cell adhesion, and metabolism (Figure S11A); cluster 1 was affected in a limited way, with only VEGFR signaling as the main enriched pathway (Figure S11B); on the contrary, cluster 2 cells were deeply affected by the treatment, even at this early time point, and most TKR pathways were significantly enriched as well as mTOR/autophagy pathways (Figures S11C and S11D).

Last, we extended our enrichment analysis to all gene signatures (GSEA) part of The Molecular Signatures Database (MSigDB) (Table S7). We found the signature "ANDERSEN_CHOLANGIOCARCINOMA_CLASS2," which collects genes overexpressed in cholangiocarcinoma class 2 associated with a poor prognosis, as negatively enriched in cluster 2 (NES -3.34, adjusted p value $8.53E^{-10}$). While the enrichment was not significant in cluster 1 (adjusted p value 0.02), the sign of the normalized enrichment score remained negative (−2.2). Similarly, "HOSHIDA_LIVER_CANCER_SUBCLASS_S1" (genes from "subtype S1" signature of hepatocellular carcinoma, linked to an aberrant activation of the WNT signaling pathway) was enriched with a negative score in cluster 1 (NES −2.4, adjusted p value $6.1E^{-3}$), and obtained a negative but not significant score in cluster 2 (NES −2.1, adjusted p value 0.02). Overall, these results hint at a role of the treatment in reducing the activity of genes involved with cancer progression.

DISCUSSION

Treatment choice for CUP patients is always challenging due to the inconclusiveness of classical diagnostic investigations in tumor type identification. In this scenario, therapy can be based on empirical approaches, molecular predictions of the primary site, the clinical assessment of the similarity with other known tumor types, or more recently, on molecularly guided approaches. Indeed, the combination of molecular and genetic investigations can help the treating clinicians to define the most probable site of origin or potential druggable mutations and use this information to choose the best therapeutic strategies.

CUP therapeutic choice has been also hampered by the lack of CUP models on which to test novel therapeutic approaches or investigate the biology of this aggressive disease. The availability of viable tumor cells is one of the main limitations in the development of CUP models. Recently, Verginelli et al. described the generation of the first CUP *in vitro* and *in vivo* models from biopsy/surgery tumor tissue, showing how they recapitulate the genetics of the original tumors and present a stem cell-like phenotype.[30] Since tumor cell proliferation in their models was sustained by constitutive activation of the

Figure 2. Single-cell transcriptome analysis of CUP#55

(A) Scores computed by the scType method for putative tissues of origin for CUP#55 cells. (B) Cell clustering based on the similarity among expression profiles, obtained through the scLCA method; cells are separated in two distinct clusters. (C) The panels show the expression and distribution in CUP#55 single cells of the FGFR2 gene and other selected markers expressed in liver cancer stem cells and involved in the EMT process.

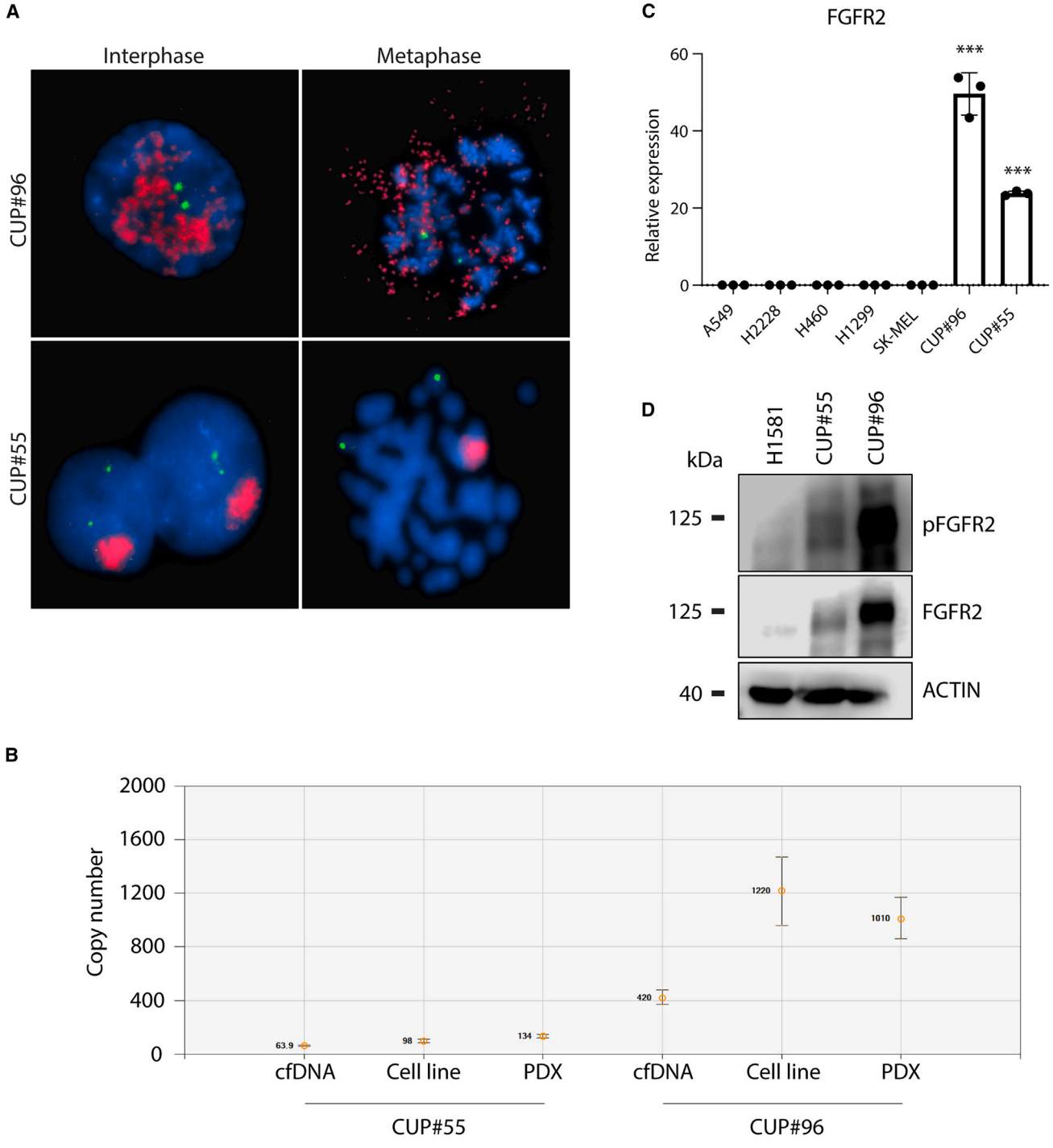

Figure 3. FGFR2 amplification in CUP models

(A) FISH analysis shows the different nature of FGFR2 amplification in the two CUP cell models: double minutes for CUP#96 and HSR for CUP#55; *FGFR2* gene probe is in red, Chr10 centromere probe in green, nucleus in blue. (B) Copy number variation (CNV) analysis of *FGFR2* gene detected by ddPCR using a probe-based assay. (C) FGFR2 gene expression in the two amplified models and a control not amplified cell line. Bars represent the relative expression of genes using HPRT as reference genes and the $2^{-\Delta Ct}$ method. Data are represented as mean ± SD. Ordinary one-way ANOVA was used, ***p <0.001. (D) Evaluation by western blot analysis of total and phosphorylated forms of FGFR2 in CUP#55 and #96, compared with the H1581 NSCLC cell line.

Please cite this article in press as: Cavazzoni et al., Synergic activity of FGFR2 and MEK inhibitors in the treatment of FGFR2-amplified cancers of unknown primary, Molecular Therapy (2024), https://doi.org/10.1016/j.ymthe.2024.07.011

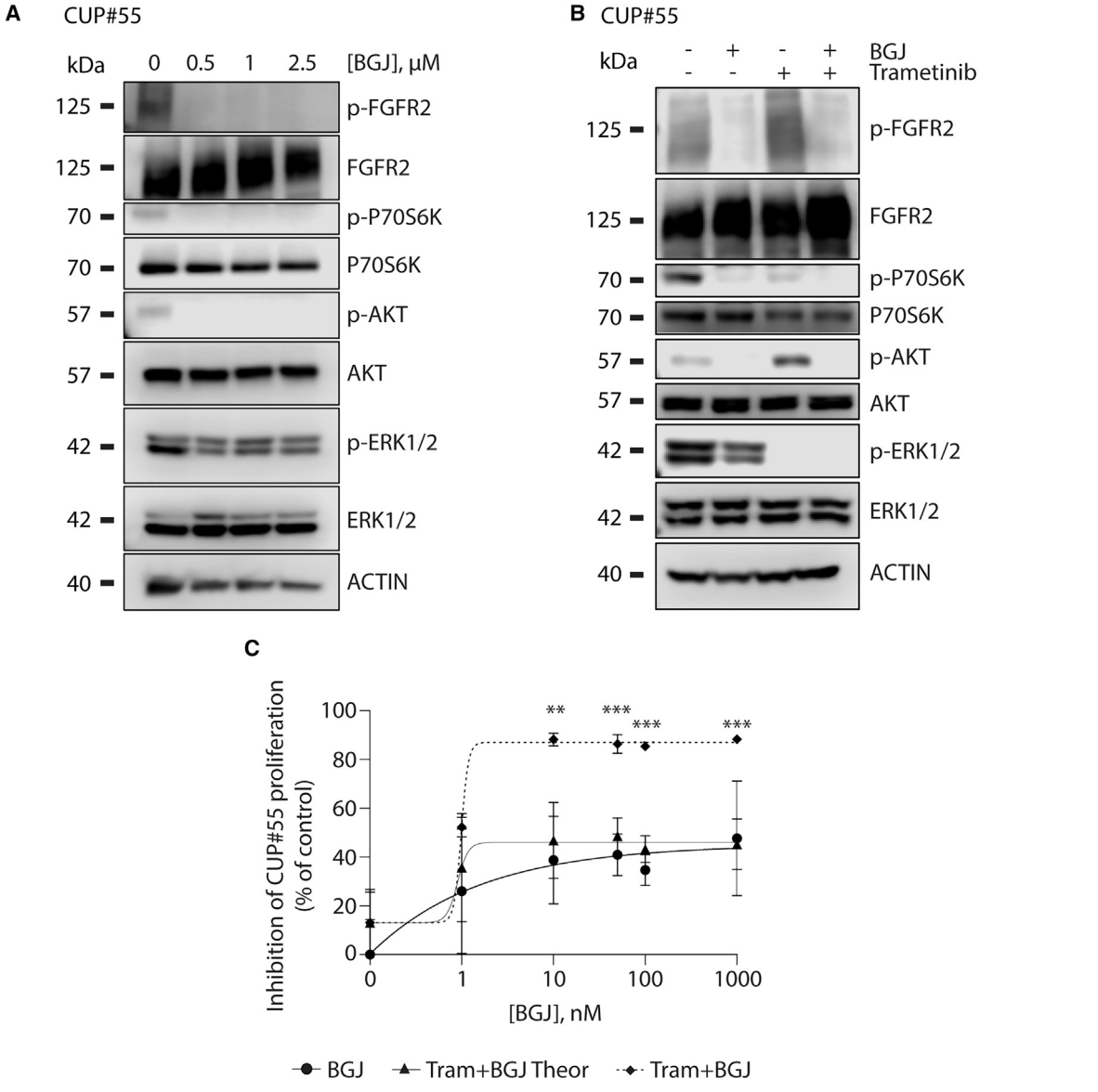

(legend on next page)

MAPK pathway, they described how the use of a MAP2K1/2 inhibitor, trametinib, strongly reduced cell viability and tumor volume in xenograft models.

Here, we described two *in vitro* and *in vivo* models we derived from ascites circulating tumors cells (CTCs) of CUP patients, named CUP#55 and CUP#96. Using a CTC-optimized protocol, we established two long-term cell cultures spontaneously growing as spheroids/tumoroids and expressing stem cell markers. Combined investigations on miRNA expression, single-cell transcriptomics, and genomic alterations pointed toward a biliary tract origin for CUP#55 and gastrointestinal origin for CUP#96.

The ascites CTCs were engrafted into mice to generate two patient-derived xenografts, which recapitulated the characteristics of the original tumor. The genetic analyses, performed on tumor tissues and models, revealed that the two models shared the *FGFR2* amplification as main genetic alteration, although of a different nature. *FGFR2* amplification is reported in several solid tumors, including gastric cancer and breast cancer,[31] while its translocation is a recurrent feature in cholangiocarcinoma.[32] *FGFR2* amplification is associated with increased levels of the protein and its aberrant phosphorylation leads to the activation of downstream pathways, including MAPK-ERK signaling,[33] which in turn accelerates cell proliferation. Since FGFR2 amplification is a druggable target,[33] we investigated the extent of CUP tumor FGFR2 dependency.

The treatment with BGJ398 (infigratinib), a pan-FGFR inhibitor, demonstrated the effectiveness of this target therapy in reducing AKT activation; in contrast, ERK1/2 phosphorylation was downregulated in the CUP#96, but not CUP#55 model, suggesting that in these cells the MAPK signaling remained active through alternative mechanisms, possibly related to NTRK1 and ERBB3 mutations. Indeed, both ERBB3 and NTRK1 mutations were previously shown to confer resistance to FGFR inhibitors by sustaining MAPK pathway activation.[34] Our findings suggest that FGFR2 targeting in FGFR2-amplified CUPs might not be sufficient to halt tumor growth, due to the concomitant activation of alternative survival/proliferation pathways. Therefore, we investigated the effect of the combined use of trametinib, an MAPK pathway inhibitor selective for MAP2K1/2. MAPK is a pathway that is frequently activated in CUPs,[35] where its activation correlates with worse prognosis. Interestingly, the combined treatment with FGFR2 and MEK inhibitors generated a remarkable synergistic effect, reducing cell growth and viability in both cell models with induction of cell death.

Mechanistically, we can speculate that trametinib acts to increase the inhibitory effect of BGJ398 on FGFR2-mediated activation of MAPK signaling in CUP#96, while in CUP#55 the two drugs seem to act separately. Indeed, the treatment with trametinib alone in CUP#55, while inhibiting MAPK signaling, increased AKT phosphorylation/activation. This effect was completely reverted by BGJ398, thus contributing to the synergistic activity of the drug combination. This finding, which was previously reported by our and other groups in other cell models,[36,37] highlights the existence of a context-dependent crosstalk between AKT and MAPK pathways and reinforces the notion that the combined inhibition of both signaling is required to achieve an effective suppression of cancer cell growth.

The single-cell transcriptomic investigation of the CUP#55 cell line, treated short-term with BGJ398 and trametinib, revealed a degree of plasticity in the apparently homogeneous cell line, which was evidenced by the presence of two main molecular phenotypes. These two CUP#55 cellular states were differentially affected by the combined treatment, with genes involved in angiogenesis and cancer metabolism being affected in both cell subgroups (clusters) and cells with a stronger epithelial phenotype (cluster 2) being more susceptible to treatment-induced cell inhibition of receptor tyrosine kinase downstream pathways.

To validate the results in a preclinical model, the corresponding PDXs were treated with the drug combination and the effect was a drastic and significant reduction of the tumor size if compared with single treatments. The treatment combination was well tolerated by the CUP#96 model but aggravated the mice frailty in the CUP#55 model, which already presented signs of tumor-induced cachexia.

In the last years, pemigatinib and infigratinib, both orally active agents targeting FGFR1-4, have received an accelerated approval by the US Food and Drug Administration (FDA) for the treatment of adult patients with previously treated and unresectable or metastatic cholangiocarcinoma harboring FGFR2 fusion or other rearrangement. Based on some concerns, the European agency (EMA) granted approval with the same indication only for pemigatinib. Likewise, erdafitinib, an orally active small potent TKI of FGFR1–4, was granted accelerated approval for patients with locally advanced or metastatic

Figure 4. *In vitro* FGFR2 targeting and synergic activity of FGFR2 and MEK inhibitors in CUP#55

(A) CUP#55 cells were treated with BGJ398 at the indicated concentrations; after 24 h, protein extracts were analyzed by western blotting for the indicated proteins. The results are representative of two independent experiments. (B) CUP#55 cells were incubated with BGJ398 1 μM, trametinib 100 nM, or the combination; after 24 h, protein extracts were analyzed by western blotting for the indicated proteins. The results are representative of two independent experiments. (C) CUP#55 cells were treated with increasing concentrations of BGJ398 in combination with trametinib 100 nM. After 96 h, cell proliferation was assessed by MTS assay. The data are expressed as percent inhibition vs. control. The asterisks indicate the statistical significance vs. the corresponding points of the Bliss Theoretical curve. The results are representative of three independent experiments. (D) CUP#55 cells were incubated with BGJ398 1 μM and/or trametinib 100 nM; after 96 h, the percentage of cell death was evaluated by fluorescence microscopy after Hoechst 33342/PI staining. The data are mean values ± SD of three independent experiments. (E) CUP#55 cells were incubated with BGJ398 1 μM and/or trametinib 100 nM; after 72 h, the cleavage of caspase-3 was assessed by western blot analysis. The result is representative of two independent experiments. $^{**}p < 0.01$; $^{***}p < 0.001$.

Please cite this article in press as: Cavazzoni et al., Synergic activity of FGFR2 and MEK inhibitors in the treatment of FGFR2-amplified cancers of unknown primary, Molecular Therapy (2024), https://doi.org/10.1016/j.ymthe.2024.07.011

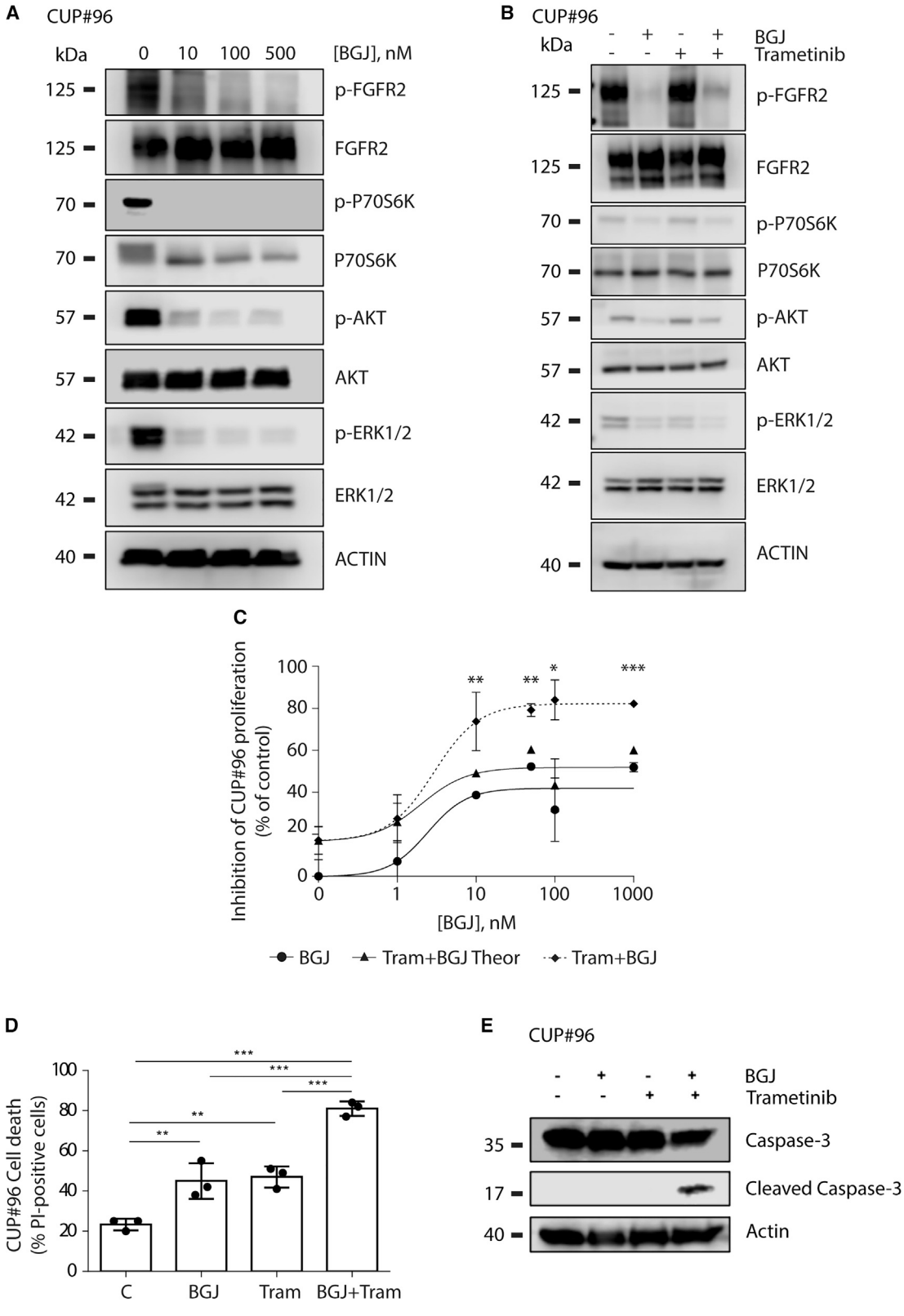

(legend on next page)

urothelial carcinoma, with susceptible FGFR3 or FGFR2 genetic alterations.

FGFR inhibitors have also been largely tested in gastric cancer patients with less enthusiastic results so far. However, positive results from a phase II trial have been reported by using bemarituzumab in addition to chemotherapy as first-line treatment for metastatic HER-2 negative gastroesophageal cancer patients with FGFR2b hyperexpression or FGFR2 gene amplification.[38] As such, several phase II and phase III trials are currently ongoing. Other new compounds, alone or in combination with other agents, are under investigation for the treatment of multiple solid tumors carrying FGFR alterations. Our results suggest that the combination of FGFR and MEK inhibitors could be a potential strategy to improve clinical outcomes in cancer patients carrying FGFR gene alterations. This means that co-targeting cross-talking pathways may potentiate FGFR inhibition, and improve the therapeutic benefit, as we have demonstrated with the MEK inhibitor trametinib.

Based on the evidence that MEK inhibition in KRAS-mutant lung cancer leads to compensatory MAPK pathway reactivation through FGFR1, combining trametinib with FGFR1-specific inhibitors encapsulated in nanoparticles allowed for efficaciously inhibiting growth and proliferation in KRAS-mutant/FGFR compensatory cancer cells.[39] In this regard, a phase 1/2 study is recruiting patients with advanced cancer of any tumor type (Part 1) or non-small cell lung cancer (NSCLC) with a confirmed KRAS mutation (Part 2) aiming at determining the recommended dose and antitumor activity of futibatinib (a selective, irreversible FGFR1-4 inhibitor) in combination with binimetinib, a known MEK inhibitor (NCT04965818).

Our study contributes to filling the gap in CUP model availability, through the generation of two human cell lines and corresponding PDXs. We demonstrated how the molecular characterization and genetic profile of the tumor can provide information to predict the most probable site of origin and identify actionable targets. In fact, the development of models that mirror the phenotype and genotype of human tumors *in vitro* and *in vivo* has become a helpful tool for drug screening, particularly to assess new therapeutic combinations that could be translated to patients with the same genetic alterations or molecular features. Indeed, the synergistic effects shown by the combination of FGFR inhibitors and MEK inhibitors *in vivo* and *in vitro* could represent the proof of concept to develop a phase 1/2 study recruiting patients with advanced cancer of unknown origin harboring FGFR amplification/activation (3% of all CUPs) with the aim of determining the recommended dose and antitumor activity of such combination. The study could be designed to also recruit patients with other tumor types characterized by FGFR2 activating genomic alterations. Although difficult to conduct due to the foreseeable recruitment, such trial would be of much interest with results that may potentially positively impact patients' outcomes.

Finally, the availability of CUP models for future studies will contribute to deepening our knowledge on the mechanisms at the base of CUP high proliferative and metastatic potential and still mysterious biology.

MATERIALS AND METHODS

Study approval

Two patients with a confirmed diagnosis of cancer of unknown primary based on European Society for Medical Oncology (ESMO) criteria (CUP#55 and CUP#96) were enrolled in this study at the Oncology Unit of IRCCS Azienda Ospedaliero-Universitaria di Bologna (Bologna, Italy). The study was approved by the local ethical committee (Comitato Etico Indipendente dell'Azienda Ospedaliero-Universitaria di Bologna, Policlinico S.Orsola Malpighi) with protocol number EM435-2022_130/2016/U/Tess/AOUBo. All subjects provided a written informed consent for study participation, in accordance with the Declaration of Helsinki.

Cell culture

NSCLC cell lines H1581, A549, H460, H2228, H1299, and SK-MEL-28 were from ATCC (Manassas, VA, USA).

Cells were cultured in RPMI-1640 medium (Corning) supplemented with 10% fetal bovine serum (Corning) and maintained under standard cell culture conditions at 37°C in a water-saturated atmosphere of 5% CO_2 in air.

Patients and ascites CTC isolation

About 100 mL of ascites from both patients was collected and immediately processed. Ascites samples were centrifuged at 600 × *g* for 10 min at 4°C and the obtained pellet was treated with 10 mL red blood cell lysis buffer (Miltenyi Biotec) for 15 min at room temperature. Then, 10 mL of specific culture medium (DMEM/F12 50:50, 2 mM glutamine, 5% Horse serum, hydrocortisone 1 μg/mL, insulin

Figure 5. *In vitro* FGFR2 targeting and synergic activity of FGFR2 and MEK inhibitors in CUP#96

(A) CUP#96 cells were treated with BGJ398 at the indicated concentrations; after 24 h, protein extracts were analyzed by western blotting for the indicated proteins. The results are representative of two independent experiments. (B) CUP#96 cells were incubated with BGJ398 100 nM, trametinib 10 nM, or the combination; after 24 h, protein extracts were analyzed by western blotting for the indicated proteins. The results are representative of two independent experiments. (C) CUP#96 cells were treated with increasing concentrations of BGJ398 in combination with trametinib 10 nM. After 96 h, cell proliferation was assessed by MTS assay. The data are expressed as percent inhibition vs. control. The asterisks indicate the statistical significance vs. the corresponding points of the Bliss Theoretical curve. The results are representative of three independent experiments. (D) CUP#96 cells were incubated with BGJ398 100 nM and/or trametinib 10 nM; after 96 h, the percentage of cell death was evaluated by fluorescence microscopy after Hoechst 33342/PI staining. The data are mean values ± SD of three independent experiments. (E) CUP#96 cells were incubated with BGJ398 100 nM and/or trametinib 10 nM; after 72 h, the cleavage of caspase-3 was assessed by western blot analysis. The result is representative of two independent experiments. $^{*}p < 0.05$; $^{**}p < 0.01$; $^{***}p < 0.001$.

Please cite this article in press as: Cavazzoni et al., Synergic activity of FGFR2 and MEK inhibitors in the treatment of FGFR2-amplified cancers of unknown primary, Molecular Therapy (2024), https://doi.org/10.1016/j.ymthe.2024.07.011

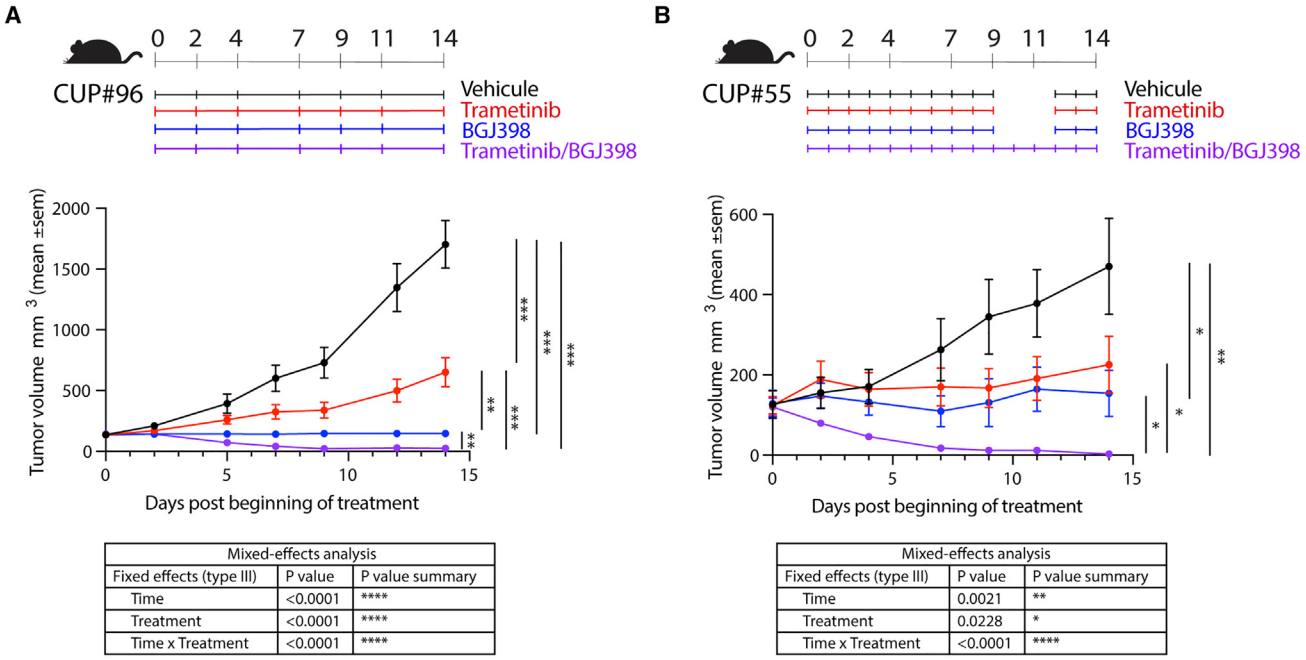

Mixed-effects analysis		
Fixed effects (type III)	P value	P value summary
Time	<0.0001	****
Treatment	<0.0001	****
Time x Treatment	<0.0001	****

Mixed-effects analysis		
Fixed effects (type III)	P value	P value summary
Time	0.0021	**
Treatment	0.0228	*
Time x Treatment	<0.0001	****

Figure 6. *In vivo* activity of FGFR2 and MEK inhibitors

In vivo treatment of (A) PDX#96 PDXs and (B) PDX#55 PDXs. The timeline shows the day of tumor volume measurement, and the color bars represent the scheme of each treatment. The line graph shows that the combination of trametinib+BGJ398 treatments (purple) is more effective than the single ones (trametinib in red and BGJ398 in blue) in both PDX models. n = 5 mice per group (mixed-effects analysis and unpaired t test were used). *$p < 0.05$; **$p < 0.01$; ***$p < 0.001$.

10 μg/mL, 1X PEN/STREP, EGF 10 ng/mL) was added and centrifuged at 600 × g for 10 min. The cells were plated in a T25 flask with 5 mL of medium in a humidified 37°C/5% CO_2 incubator. Medium was changed every 3–4 days. After 10 days, tumor cells began to grow as tumoroids (CUP#96) and spheroids (CUP#55).

Organoids and aggregates were propagated in 24-well plates to monitor growth and every 3–4 days were split 1:2. Long-term CTC cell lines were established: i.e., the cell lines were still viable after thawing cycle and showed a stable growth in medium without supplement.[40]

Pathological and immunofluorescence analysis

Cell lines, human and PDX tumor tissues were fixed in 4% paraformaldehyde for 20 min, embedded in paraffin and frozen at −20°C for optimal cutting. Sections of 4 μm were mounted on positively charged microscope slides. Sections were deparaffinized in xylene and rehydrated in graded alcohol. Antigen enhancement was done by incubating the sections in Concentrated Antigen Retrival Solution Citra Plus (BioGenex #HK080-5K) (1:10) as recommended by the manufacturer and blocked with Ventana Antibody Diluent with Casein (Roche-Ventana) for 30 min. For immunohistochemistry: Rabbit Monoclonal Primary Antibody Cytokeratin 7 (SP52) (Roche-Ventana) and Rabbit Monoclonal Primary Antibody Cytokeratin 20 (SP33) (Roche-Ventana) were used at 1:2 dilution for cell lines, human and PDX tumor tissue staining.

For immunofluorescence experiment: Mouse Monoclonal Primary Antibody CD44 (or HCAM) sc-7297 (SantaCruz) 1:100 dilution and Mouse Monoclonal Primary Antibody EPCAM FITC (REA764) (Miltenyi) 1:100 dilution was used for cell line staining. All the antibodies were incubated overnight at 4°C. Abcam Goat Anti-Rabbit IgG H&L (DyLight 594) (ab96885) and Donkey Anti-Mouse IgG H&L (DyLight 488) (ab96875)-labeled secondary antibodies were used at 1:100 dilution and incubated 1 h. Nuclei were counterstained with 1 μg/mL of Hoechst 33342 (Life Technologies). Confocal images were acquired on a Nikon A1 confocal laser scanning microscope, equipped with a ×60, 1.4 NA objective and with 405, 488-nm laser lines controlled by NIS-Elements software (Nikon) and presented as maximum intensity projection (MIP).

Genetic analysis

We used a custom 1.2-Mb SureSelect capture bait library (Agilent Technologies, Santa Clara, CA) for the target enrichment of 92 genes (panel description in Laprovitera et al.[20]). Briefly, libraries were prepared using 50 ng of genomic DNA (gDNA) input following SureSelectXT HS/SureSelectXT Low Input Target Enrichment with Pre-Capture Pooling protocol (G9702-90005, v. A0, June 2019, Agilent Technologies) and sequenced on the NextSeq 500 (Illumina) platform using High Output 2 × 75-base pair (bp) flow cells. The percentage of covered regions with zero coverage was <2% (range 0.3–1.75). Variant calling and paired analyses (tumor vs. normal) were performed using SureCall software (v. 4.2), applying a filter for tumor/normal tissue/models at 5% and for ccfDNA at 1%. Variants

Please cite this article in press as: Cavazzoni et al., Synergic activity of FGFR2 and MEK inhibitors in the treatment of FGFR2-amplified cancers of unknown primary, Molecular Therapy (2024), https://doi.org/10.1016/j.ymthe.2024.07.011

were annotated using ANNOVAR[41] and filtered to keep somatic exonic non-synonymous single-nucleotide variants (SNVs), insertions, deletions, multiple nucleotide variants, or long deletions not detected in the normal sample that presented an allele frequency in a non-Finnish European (NFE) population lower than 0.5% (Genome Aggregation Database, GnomAD[42]) and a coverage higher than 100. Bioinformatic pathogenicity prediction of the identified variants was performed consulting the prediction score/outcome of eight prediction models (Tables 1 and 2): SIFT (Sort Intolerated From Tolerated[43]), Polyphen2 HVAR (Polymorphism Phenotyping v2[44]), LRT (Likelihood Ratio Test[45]), Mutation Taster,[46] Mutation Assessor,[47] FATHMM (Functional Analysis Through Hidden Markov Model[48]), CADD (Combined Annotation Dependent Depletion[49]), and VEST (Variant Effect Scoring Tool[50]). Variants were considered pathogenic when more than 50% of the above-mentioned predictors indicated it as pathogenic/damaging/deleterious/harmful.

Single-cell transcriptome analysis

The transcriptome of the CUP#55 cell line was characterized at the single-cell level using the 10X Single-Cell 5′ R2-only kit (10X Genomics). The resulting libraries were sequenced with the Novaseq 6000 (Illumina) platform using a 2 × 100-bp flow cell (Illumina), obtaining a total yield of 240 million reads. Gene expression profiles of different cells were quantified by the CellRanger pipeline (version 7.1.0), using as a reference the GENCODE annotation (version 40). The software provided an initial estimate of 23,994 sampled cells. Gene counts were filtered by means of the CellBender method[51] to remove the confounding effects of ambient RNA molecules and random barcode swapping. Around 7% of all droplets were identified by scDblFinder[52] (version 1.14.0) as potential doublet artifacts and were excluded from the rest of the analysis. We also discarded cells characterized by a high proportion of reads from the mitochondrial genome, a signal usually associated with cell membrane rupture and apoptosis. We set our filtering threshold to 50% following the indications of other studies[53] that have observed very high mitochondrial content in hepatocytes. As a last QC filter, we dropped all cells showing a detectable level of expression for less than 500 genes. The final working set consisted of 1,437 cells.

Gene expression was loaded in the R environment using Seurat[54] (version 4.3.0.1) and normalized with the sctransform[55] method (v2) to account for gene overdispersion. Cells were clustered using the Latent Cellular Analysis method[56] (scLCA package, version 0.0.0.9000), which combines a cosine-similarity measure with a graph-based algorithm to automatically identify distinct cell subpopulations. Automatic inference of the tissue type was performed with scType[57] (version 1.0). Reference-based classification of cells was then performed using the Azimuth software[54] (version 0.4.6) and relied on its integrated atlas of the human liver.

We applied the MAST software[58] to identify marker genes of cell clusters. This method (version 1.24.0) implements a generalized linear model specifically designed to account for nuisance variation in scRNA-sequencing data. We filtered differential expression calls by setting a false discovery rate (FDR) threshold of 10^{-3}, and we also discarded all genes whose log2 fold-change was below 0.2.

Functional analysis of the resulting gene lists was performed using MetaCore analytical software (Clarivate).

Single-cell transcriptome of treated cells

We profiled the transcriptome of CUP#55 cells treated with MEK and FGFR2 inhibitors for 12 h using the single-cell protocol described above. Illumina sequencing resulted in 260 million reads, providing a reliable readout for 1,789 cells after the application of quality control filters. The shift in gene expression between treated and untreated cells was evaluated for all cells and separately for each cluster using MAST software and setting an FDR cutoff of 10^{-3} and a log fold-change cutoff at 0.02.

After obtaining the list of DEGs, we used the clusterProfiler package (version 4.10.1) to perform an enrichment analysis of WikiPathways and KEGG pathways. Resulting p values were corrected for multiple testing using the Benjamini-Hochberg procedure, and only hits with a q value ≤ 0.05 were selected.

We employed fgsea (version 1.24.0)[59] to perform a gene set enrichment analysis. Gene signatures were retrieved using msigdb (Bhuva D, Smyth G, Garnham A (2022). _msigdb: An ExperimentHub Package for the Molecular Signatures Database [MSigDB] 10.18129/B9.bioc.msigdb package version 1.6.0, database version 7.5). We downloaded an additional collection of gene sets specifically related to the epithelial-mesenchymal transition from the EMTome database[60] (data retrieved on May 3, 2023). We finally filtered fgsea results by placing an upper threshold of 10^{-2} on the Benjamini-Hochberg adjusted p values.

MicroRNA profiling

MicroRNAs (n = 89) were quantified in CUP cell lines, PDX and FFPE tumor tissue using custom miRCURY LNA miRNA plates (Qiagen) designed for CUP primary site prediction.[10] EvaGreen-based droplet digital PCR was performed as described in Laprovitera et al.[23] The miRNA-based CUP primary site prediction was performed using LASSO and PAMR algorithms as described in Laprovitera et al.[10]

Gene expression analysis with droplet digital PCR and quantitative RT-PCR

RNA was extracted from two CUP cell lines and five cancer cell lines (A549, H2228, H460, H1299, SKMEL); 500 ng of RNA for each cell line was reverse-transcribed to cDNA using iSRCIPT cDNA Synthesis Kit (Cat. No. 1708891 Bio-Rad, USA). The expression of *CD44*, *NANOG*, *POU5F1*, and *FGFR2* was quantified using reverse transcription quantitative PCR (RT-qPCR) or QX200 Droplet Digital PCR system (Bio-Rad, Hercules, CA, USA). SsoAdvanced Universal SYBR Green Supermix (Cat. No. 1725271 Bio-Rad, USA) was used and raw Cq values were obtained from Bio-Rad CFX Maestro 2.2 software (version 5.2.008.0222) for the calculation of relative expression

using $2^{-\Delta Ct}$ method using HPRT as reference gene. Bio-Rad EvaGreen protocol for gene expression quantification was used to quantify the gene copies per ng of cDNA by QuantaSoft Analysis software (Bio-Rad, Hercules, CA, USA). HPRT was used as a reference gene to normalize (ratio gene/reference) the gene expression. The primers used for the gene expression analysis are reported below:

CD44 F: ATGAGGGATATCGCCAAACA.

CD44 R: GGTGTTGTCCTTCCTTGCAT.

NANOG F: TTTGTGGGCCTGAAGAAAACT.

NANOG R: AGGGCTGTCCTGAATAAGCAG.

POU5F1 F: GGGTTCTATTTGGGAAGGTAT.

POU5F1 R: TTCATTGTTGTCAGCTTCCT.

FGFR2 F: CAGGGGTCTCCGAGTATGAA.

FGFR2 R: TCCTTGGGCTTGTCTTTGTC.

HPRT F: TGACACTGGCAAAACAATGCA.

HPRT R: GGTCCTTTTCACCAGCAAGCT.

FGFR2b_Ex7-8_F TCTCAAGCACTCGGGGATAA.

FGFR2b_Ex7-8_R TGTTTTGGCAGGACAGTGAG.

FGFR2c_Ex7-8_F TGCCCTACCTCAAGGTTCTC.

FGFR2c_Ex7-8_R CAACCATGCAGAGTGAAAGG.

Fluorescence *in situ* hybridization

FISH analysis was performed on fixed CUP#55 and CUP#96 interphase nuclei and metaphases. Two Empire Genomics probes (Empire Genomics, Buffalo, NY) were employed following the manufacturer's protocol. Specifically, the FGFR2 gene probe (orange) maps on chr:10q26.13 and the CEP10 probe maps to the centromeric region of chromosome 10. CUP#55 and CUP#96 cells were counterstained with 4',6-diamidino-2-phenylindole (DAPI) for nuclear detection. Analysis was performed using Olympus BX53 microscopy equipped with the appropriate filter sets and CytoVision software (Leica Biosystems, Nussloch, Germany).

Detection of *FGFR2* amplification

Total DNA was extracted from CUP#55 and CUP#96 cell lines and PDXs using QIAamp DNA Mini Kit (Cat. No. 5130450, Qiagen). Cell-free DNA was extracted from 1 mL plasma with Maxwell RSC ccfDNA Plasma Kit (Cat No: AS1480, Promega). Tumor DNA was extracted using the QIAamp DNA FFPE Tissue Kit (Cat No: 56404, Qiagen, Hilden, Germany). To quantify the CN of *FGFR2* in all samples, a probe-based droplet digital PCR assay was used. *RPP30* was tested as the reference gene for diploid CN. RPP30 probe (dHsaCP2500350, Bio-Rad) was labeled with HEX, and FGFR2 probe (dHsaCB2500320) was labeled with FAM. Droplet digital PCR was performed with the QX200 Droplet Digital PCR system (Bio-Rad, USA) as described in Laprovitera et al.[20] *FGFR2* gene CN was calculated by QuantaSoft Analysis software (Bio-Rad, Hercules, CA, USA) as *FGFR2/RPP30* ratio.

Cell viability and drug response assays

Cell viability/proliferation was evaluated by a CellTiter-Glo 96 Aqueous One solution assay (Promega). Cell death was analyzed by (1) fluorescence microscopy after staining with Hoechst 3342 and propidium iodide (PI)[61]; (2) western blot analysis of caspase-3 cleavage; (3) flow cytometry after Annexin V-FITC and PI staining (Annexin V-FITC apoptosis detection kit, Thermo Fisher) using a Cytoflex flow cytometer (Beckman Coulter, Brea, CA, USA) for acquisition and the Beckman Coulter's Kaluza software for subsequent analysis. BGJ398 (infigratinib) and trametinib (mekinist) were purchased from Selleckchem (Houston, TX), and dissolved in DMSO. DMSO concentration never exceeded 0.1% (v/v); equal amounts of the solvent were added to control cells. The effect of the drug combination was evaluated using the Bliss interaction model.[62]

Western blotting

For western blot analysis, 8×10^5 cells from CUP#55 or CUP#96 were seeded in six-well-plates in complete culture medium. At the end of the treatments, the cells were harvested and centrifuged. The procedures for protein extraction, solubilization, and protein analysis by western blotting are described elsewhere.[63] Antibodies against *p*-FGFR (#3471), FGFR2 (#11835), *p*-ERK1/2$^{Thr202/Tyr204}$ (#4370), ERK1/2 (#4695), *p*-AKT^{Ser473} (#9271), AKT (#9272), *p*-P70S6K^{Thr389} (#9205), P70S6K (#9202), and caspase-3 (#9662) were from Cell Signaling Technology, Incorporated (Danvers, MA); anti-β-actin (clone B11V08) was from BioVision (Milpitas, CA). Horseradish peroxidase-conjugated secondary antibodies and the chemiluminescence system were from Millipore (Millipore, MA). Reagents for electrophoresis and blotting analysis were from Bio-Rad Laboratories (Hercules, CA). The chemiluminescent signal was acquired by C-DiGit R Blot Scanner and the bands were quantified by Image StudioTMSoftware, LI-COR Biotechnology (Lincoln, NE).

Growth of CUP tumors in immunocompromised mice

PDX studies were run at XenTech in compliance with authorization n. APAFIS#30365–2021012215599431 v1 conferred from the French Ministry of Agriculture and Food. The authorization to use animals in the CERFE facility (Evry-Courcouronne, France) was obtained by The Direction Départementale de la Protection des Populations, Ministère de l'Agriculture et de l'Alimentation, France "Direction of the Veterinarian Services, Ministry of Agriculture and Food, France" (agreement No. D-91-228-107).

An approximate number of 3–4,000 cells or 30–40 organoids were resuspended in 100 μL of culture medium, diluted 1:1 in matrigel and grafted in the interscapular region of NOD/Scid-IL2Rγ−/− (NSG) or NOD/Shi-scid/IL-2Rγnull (NOG) mice. Tumor fragments were sampled from the resected tumor, minced on ice, and immediately placed in MACS Tissue Storage Solution (Miltenyi Biotech) and transferred to the animal facility, fragmented and grafted in the interscapular region of Athymic Nude-Foxn1nu mice. Mice were monitored twice weekly for signs of tumor growth. Tumor growth from first implantation occurred in 135 days for CUP#55 and 40 days for CUP#96. Growing tumors were serially transplanted onto recipient mice and the fragments of the tumor harvested for IHC analysis, and DNA and RNA extraction. To immortalize each PDX, vials of tumor fragments at different passages were placed in 90% FCS/10% DMSO or glycerol, and stored at −150°C.

In vivo treatments

Treatment efficacy studies on each PDX were run as follows. Tumor fragments of the same passage were transplanted subcutaneously onto 3–24 mice (donor mice). When the tumors reached 700 to 1,764 mm^3, donor mice were euthanized, and tumors were cut into fragments measuring approximately 20 mm^3. Mice aged 8 to 11 weeks were anesthetized with 100 mg/kg ketamine hydrochloride and 10 mg/kg xylazine, and one tumor fragment was placed in the interscapular fat pad. On the day of enrollment in the study, mice with tumor volume ranging 60 to 200 mm^3 were randomly attributed to the different groups reported in Table S8. From day 12 to day 14, half dose was administered due to body weight loss.

Trametinib was purchased at Carbosynth and suspended in 10% DMSO; 40% PEG300; 5% Tween-80; 45% NaCl 0.9% for administration; BGJ398 (infigratinib) was purchased at MedChem Express and diluted in 50% acetic acid/acetate buffer/50% PEG300 for administration. Tumor volume was evaluated by measuring tumor diameters with a caliper, three times a week during the treatment period (from D0 to D27); all animals were weighed, and tumor size measured the same day. During the whole experimental period, animals were monitored every day for physical appearance, behavior, and clinical changes.

STATISTICAL ANALYSIS

Statistical analyses were carried out using GraphPad Prism v. 10.00 software. Unpaired t test was used for two-group comparisons, ordinary one-way ANOVA for multiple comparisons, and two-way ANOVA (mixed-effects analysis) for the time + treatment analysis of PDX treatment data. The number of replicates or independent experiments is reported in the figure legends. A two-sided p value less than 0.05 was considered significant ($^*p < 0.05$; $^{**}p < 0.01$; $^{***}p < 0.001$). Data are represented as mean ± standard deviation (SD).

DATA AND CODE AVAILABILITY

Processed single-cell transcriptomic data and microRNA expression data are available as supplementary information. Genomic and single-cell transcriptomic raw data are available from the authors upon request.

SUPPLEMENTAL INFORMATION

Supplemental information can be found online at https://doi.org/10.1016/j.ymthe.2024.07.011.

ACKNOWLEDGMENTS

The research leading to these results has received funding from Fondazione Italiana per la Ricerca sul Cancro AIRC grant IG 2021 - ID. 25789 to M.F., Pallotti Institutional funds to M.F., Fondazione del Monte to M.F., and UNIPD PRID 2019 – ID. BIRD193023 to G.S. Graphical abstract was created with BioRender.com.

AUTHOR CONTRIBUTIONS

Conceptualization: A.C., G.S., and M.F.; Methodology: E.P., S.C., G.S., A.C., I.S., and M.F.; Investigation: A.C., C.F., I.S., N.L., G.G., M.R., M.N., S.S., E.B., G.D., R.R., and I.P.; Funding Acquisition: M.F.; Resources: F.G., K.R., M.L., I.G., A.D., O.D., P.G.P., A.A., G.S., and M.F.; Writing-Original Draft: A.C., I.S., C.F., G.S., and M.F.; Writing-Review & Editing: G.A.C., M.B., A.A., F.G., G.S., and M.F.

DECLARATION OF INTERESTS

F.G. received personal fees from AstraZeneca and honoraria for advisory board participation from Eli-Lilly. G.A.C. is a member of the Editorial Board of Molecular Therapy.

REFERENCES

1. Chaffer, C.L., and Weinberg, R.A. (2011). A perspective on cancer cell metastasis. Science *331*, 1559–1564. https://doi.org/10.1126/science.1203543.

2. Varadhachary, G.R., and Raber, M.N. (2014). Cancer of unknown primary site. N. Engl. J. Med. *371*, 757–765. https://doi.org/10.1056/NEJMra1303917.

3. Laprovitera, N., Riefolo, M., Ambrosini, E., Klec, C., Pichler, M., and Ferracin, M. (2021). Cancer of Unknown Primary: Challenges and Progress in Clinical Management. Cancers (Basel) *13*, 451. https://doi.org/10.3390/cancers13030451.

4. Warner, E., Goel, R., Chang, J., Chow, W., Verma, S., Dancey, J., Franssen, E., Dulude, H., Girouard, M., Correia, J., and Gallant, G. (1998). A multicentre phase II study of carboplatin and prolonged oral etoposide in the treatment of cancer of unknown primary site (CUPS). Br. J. Cancer *77*, 2376–2380. https://doi.org/10.1038/bjc.1998.395.

5. Pentheroudakis, G., Briasoulis, E., Kalofonos, H.P., Fountzilas, G., Economopoulos, T., Samelis, G., Koutras, A., Karina, M., Xiros, N., Samantas, E., et al. (2008). Docetaxel and carboplatin combination chemotherapy as outpatient palliative therapy in carcinoma of unknown primary: a multicentre Hellenic Cooperative Oncology Group phase II study. Acta Oncol. *47*, 1148–1155. https://doi.org/10.1080/02841860701843043.

6. Briasoulis, E., Fountzilas, G., Bamias, A., Dimopoulos, M.A., Xiros, N., Aravantinos, G., Samantas, E., Kalofonos, H., Makatsoris, T., Mylonakis, N., et al. (2008). Multicenter phase-II trial of irinotecan plus oxaliplatin [IROX regimen] in patients with poor-prognosis cancer of unknown primary: a hellenic cooperative oncology group study. Cancer Chemother. Pharmacol. *62*, 277–284. https://doi.org/10.1007/s00280-007-0604-7.

7. Huebner, G., Link, H., Kohne, C.H., Stahl, M., Kretzschmar, A., Steinbach, S., Folprecht, G., Bernhard, H., Al-Batran, S.E., Schoffski, P., et al. (2009). Paclitaxel and carboplatin vs gemcitabine and vinorelbine in patients with adeno- or undifferentiated carcinoma of unknown primary: a randomised prospective phase II trial. Br. J. Cancer *100*, 44–49. https://doi.org/10.1038/sj.bjc.6604818.

8. Hainsworth, J.D., Spigel, D.R., Clark, B.L., Shipley, D., Thompson, D.S., Farley, C., West-Osterfield, K., Lane, C.M., Cescon, T., Bury, M.J., and Greco, F.A. (2010).

Paclitaxel/carboplatin/etoposide versus gemcitabine/irinotecan in the first-line treatment of patients with carcinoma of unknown primary site: a randomized, phase III Sarah Cannon Oncology Research Consortium Trial. Cancer J. *16*, 70–75. https://doi.org/10.1097/PPO.0b013e3181c6aa89.

9. Gross-Goupil, M., Fourcade, A., Blot, E., Penel, N., Négrier, S., Culine, S., Chaigneau, L., Lesimple, T., Priou, F., Lortholary, A., et al. (2012). Cisplatin alone or combined with gemcitabine in carcinomas of unknown primary: results of the randomised GEFCAPI 02 trial. Eur. J. Cancer *48*, 721–727. https://doi.org/10.1016/j.ejca.2012.01.011.

10. Laprovitera, N., Riefolo, M., Porcellini, E., Durante, G., Garajova, I., Vasuri, F., Aigelsreiter, A., Dandachi, N., Benvenuto, G., Agostinis, F., et al. (2021). MicroRNA expression profiling with a droplet digital PCR assay enables molecular diagnosis and prognosis of cancers of unknown primary. Mol. Oncol. *15*, 2732–2751. https://doi.org/10.1002/1878-0261.13026.

11. Hayashi, H., Takiguchi, Y., Minami, H., Akiyoshi, K., Segawa, Y., Ueda, H., Iwamoto, Y., Kondoh, C., Matsumoto, K., Takahashi, S., et al. (2020). Site-Specific and Targeted Therapy Based on Molecular Profiling by Next-Generation Sequencing for Cancer of Unknown Primary Site: A Nonrandomized Phase 2 Clinical Trial. JAMA Oncol. *6*, 1931–1938. https://doi.org/10.1001/jamaoncol.2020.4643.

12. Clynick, B., Dessauvagie, B., Sterrett, G., Harvey, N.T., Allcock, R.J.N., Saunders, C., Erber, W., and Meehan, K. (2018). Genetic characterisation of molecular targets in carcinoma of unknown primary. J. Transl. Med. *16*, 185. https://doi.org/10.1186/s12967-018-1564-x.

13. Ross, J.S., Wang, K., Gay, L., Otto, G.A., White, E., Iwanik, K., Palmer, G., Yelensky, R., Lipson, D.M., Chmielecki, J., et al. (2015). Comprehensive Genomic Profiling of Carcinoma of Unknown Primary Site: New Routes to Targeted Therapies. JAMA Oncol. *1*, 40–49. https://doi.org/10.1001/jamaoncol.2014.216.

14. Varghese, A.M., and Saltz, L.B. (2015). Genomic Profiling of Cancers of Unknown Primary Site: The Next Steps. JAMA Oncol. *1*, 541–542. https://doi.org/10.1001/jamaoncol.2015.0939.

15. Zehir, A., Benayed, R., Shah, R.H., Syed, A., Middha, S., Kim, H.R., Srinivasan, P., Gao, J., Chakravarty, D., Devlin, S.M., et al. (2017). Mutational landscape of metastatic cancer revealed from prospective clinical sequencing of 10,000 patients. Nat. Med. *23*, 703–713. https://doi.org/10.1038/nm.4333.

16. AACR Project GENIE Consortium (2017). AACR Project GENIE: Powering Precision Medicine through an International Consortium. Cancer Discov. *7*, 818–831. https://doi.org/10.1158/2159-8290.CD-17-0151.

17. Lombardo, R., Tosi, F., Nocerino, A., Bencardino, K., Gambi, V., Ricotta, R., Spina, F., Siena, S., and Sartore-Bianchi, A. (2020). The Quest for Improving Treatment of Cancer of Unknown Primary (CUP) Through Molecularly-Driven Treatments: A Systematic Review. Front. Oncol. *10*, 533. https://doi.org/10.3389/fonc.2020.00533.

18. Gatalica, Z., Xiu, J., Swensen, J., and Vranic, S. (2018). Comprehensive analysis of cancers of unknown primary for the biomarkers of response to immune checkpoint blockade therapy. Eur. J. Cancer *94*, 179–186. https://doi.org/10.1016/j.ejca.2018.02.021.

19. Ding, Y., Jiang, J., Xu, J., Chen, Y., Zheng, Y., Jiang, W., Mao, C., Jiang, H., Bao, X., Shen, Y., et al. (2022). Site-specific therapy in cancers of unknown primary site: a systematic review and meta-analysis. ESMO Open *7*, 100407. https://doi.org/10.1016/j.esmoop.2022.100407.

20. Laprovitera, N., Salamon, I., Gelsomino, F., Porcellini, E., Riefolo, M., Garonzi, M., Tononi, P., Valente, S., Sabbioni, S., Fontana, F., et al. (2021). Genetic Characterization of Cancer of Unknown Primary Using Liquid Biopsy Approaches. Front. Cel Dev. Biol. *9*, 666156. https://doi.org/10.3389/fcell.2021.666156.

21. Pouyiourou, M., Bochtler, T., Coith, C., Wikman, H., Kraft, B., Hielscher, T., Stenzinger, A., Riethdorf, S., Pantel, K., and Krämer, A. (2024). Frequency and Prognostic Value of Circulating Tumor Cells in Cancer of Unknown Primary. Clin. Chem. *70*, 297–306. https://doi.org/10.1093/clinchem/hvad180.

22. Janik, K., Popeda, M., Peciak, J., Rosiak, K., Smolarz, M., Treda, C., Rieske, P., Stoczynska-Fidelus, E., and Ksiazkiewicz, M. (2016). Efficient and simple approach to in vitro culture of primary epithelial cancer cells. Biosci. Rep. *36*, e00423. https://doi.org/10.1042/BSR20160208.

23. Laprovitera, N., Grzes, M., Porcellini, E., and Ferracin, M. (2018). Cancer Site-Specific Multiple microRNA Quantification by Droplet Digital PCR. Front. Oncol. *8*, 447. https://doi.org/10.3389/fonc.2018.00447.

24. Pugh, T.J., Bell, J.L., Bruce, J.P., Doherty, G.J., Galvin, M., Green, M.F., Hunter-Zinck, H., Kumari, P., Lenoue-Newton, M.L., Li, M.M., et al. (2022). AACR Project GENIE: 100,000 Cases and Beyond. Cancer Discov. *12*, 2044–2057. https://doi.org/10.1158/2159-8290.CD-21-1547.

25. Gong, S.G. (2014). Isoforms of receptors of fibroblast growth factors. J. Cel. Physiol. *229*, 1887–1895. https://doi.org/10.1002/jcp.24649.

26. Orr-Urtreger, A., Bedford, M.T., Burakova, T., Arman, E., Zimmer, Y., Yayon, A., Givol, D., and Lonai, P. (1993). Developmental localization of the splicing alternatives of fibroblast growth factor receptor-2 (FGFR2). Dev. Biol. *158*, 475–486. https://doi.org/10.1006/dbio.1993.1205.

27. SenthilKumar, G., Fisher, M.M., Skiba, J.H., Miller, M.C., Brennan, S.R., Kaushik, S., Bradley, S.T., Longhurst, C.A., Buehler, D., Nickel, K.P., et al. (2020). FGFR Inhibition Enhances Sensitivity to Radiation in Non-Small Cell Lung Cancer. Mol. Cancer Ther. *19*, 1255–1265. https://doi.org/10.1158/1535-7163.MCT-19-0931.

28. Tan, T.Z., Miow, Q.H., Miki, Y., Noda, T., Mori, S., Huang, R.Y.J., and Thiery, J.P. (2014). Epithelial-mesenchymal transition spectrum quantification and its efficacy in deciphering survival and drug responses of cancer patients. EMBO Mol. Med. *6*, 1279–1293. https://doi.org/10.15252/emmm.201404208.

29. Cursons, J., Leuchowius, K.J., Waltham, M., Tomaskovic-Crook, E., Foroutan, M., Bracken, C.P., Redfern, A., Crampin, E.J., Street, I., Davis, M.J., and Thompson, E.W. (2015). Stimulus-dependent differences in signalling regulate epithelial-mesenchymal plasticity and change the effects of drugs in breast cancer cell lines. Cell Commun. Signal. *13*, 26. https://doi.org/10.1186/s12964-015-0106-x.

30. Verginelli, F., Pisacane, A., Gambardella, G., D'Ambrosio, A., Candiello, E., Ferrio, M., Panero, M., Casorzo, L., Benvenuti, S., Cascardi, E., et al. (2021). Cancer of unknown primary stem-like cells model multi-organ metastasis and unveil liability to MEK inhibition. Nat. Commun. *12*, 2498. https://doi.org/10.1038/s41467-021-22643-w.

31. Katoh, M. (2008). Cancer genomics and genetics of FGFR2 (Review). Int. J. Oncol. *33*, 233–237.

32. Smyth, E.C., Babina, I.S., and Turner, N.C. (2017). Gatekeeper Mutations and Intratumoral Heterogeneity in FGFR2-Translocated Cholangiocarcinoma. Cancer Discov. *7*, 248–249. https://doi.org/10.1158/2159-8290.CD-17-0057.

33. Babina, I.S., and Turner, N.C. (2017). Advances and challenges in targeting FGFR signalling in cancer. Nat. Rev. Cancer *17*, 318–332. https://doi.org/10.1038/nrc.2017.8.

34. Bockorny, B., Rusan, M., Chen, W., Liao, R.G., Li, Y., Piccioni, F., Wang, J., Tan, L., Thorner, A.R., Li, T., et al. (2018). RAS-MAPK Reactivation Facilitates Acquired Resistance in FGFR1-Amplified Lung Cancer and Underlies a Rationale for Upfront FGFR-MEK Blockade. Mol. Cancer Ther. *17*, 1526–1539. https://doi.org/10.1158/1535-7163.MCT-17-0464.

35. Krikelis, D., Pentheroudakis, G., Goussia, A., Siozopoulou, V., Bobos, M., Petrakis, D., Stoyianni, A., Golfinopoulos, V., Cervantes, A., Ciuleanu, T., et al. (2012). Profiling immunohistochemical expression of NOTCH1-3, JAGGED1, cMET, and phospho-MAPK in 100 carcinomas of unknown primary. Clin. Exp. Metastasis *29*, 603–614. https://doi.org/10.1007/s10585-012-9474-4.

36. Fumarola, C., Bozza, N., Castelli, R., Ferlenghi, F., Marseglia, G., Lodola, A., Bonelli, M., La Monica, S., Cretella, D., Alfieri, R., et al. (2019). Expanding the Arsenal of FGFR Inhibitors: A Novel Chloroacetamide Derivative as a New Irreversible Agent With Anti-proliferative Activity Against FGFR1-Amplified Lung Cancer Cell Lines. Front. Oncol. *9*, 179. https://doi.org/10.3389/fonc.2019.00179.

37. Malchers, F., Ercanoglu, M., Schütte, D., Castiglione, R., Tischler, V., Michels, S., Dahmen, I., Brägelmann, J., Menon, R., Heuckmann, J.M., et al. (2017). Mechanisms of Primary Drug Resistance in FGFR1-Amplified Lung Cancer. Clin. Cancer Res. *23*, 5527–5536. https://doi.org/10.1158/1078-0432.CCR-17-0478.

38. Wainberg, Z.A., Enzinger, P.C., Kang, Y.K., Qin, S., Yamaguchi, K., Kim, I.H., Saeed, A., Oh, S.C., Li, J., Turk, H.M., et al. (2022). Bemarituzumab in patients with FGFR2b-selected gastric or gastro-oesophageal junction adenocarcinoma (FIGHT): a randomised, double-blind, placebo-controlled, phase 2 study. Lancet Oncol. *23*, 1430–1440. https://doi.org/10.1016/S1470-2045(22)00603-9.

39. Izawa-Ishiguro, A.R., Sridharan, R., Wun, C., Sami, T.J., and Heller, D.A. (2022). Abstract 302: MEKi-FGFRi combination nanoparticles for use against KRASmt/FGFR-compensatory lung tumors. Cancer Res. *82*, 302. https://doi.org/10.1158/1538-7445.Am2022-302.

40. Kodack, D.P., Farago, A.F., Dastur, A., Held, M.A., Dardaei, L., Friboulet, L., von Flotow, F., Damon, L.J., Lee, D., Parks, M., et al. (2017). Primary Patient-Derived Cancer Cells and Their Potential for Personalized Cancer Patient Care. Cell Rep. *21*, 3298–3309. https://doi.org/10.1016/j.celrep.2017.11.051.

41. Wang, K., Li, M., and Hakonarson, H. (2010). ANNOVAR: functional annotation of genetic variants from high-throughput sequencing data. Nucleic Acids Res. *38*, e164. https://doi.org/10.1093/nar/gkq603.

42. Karczewski, K.J., Francioli, L.C., Tiao, G., Cummings, B.B., Alföldi, J., Wang, Q., Collins, R.L., Laricchia, K.M., Ganna, A., Birnbaum, D.P., et al. (2020). The mutational constraint spectrum quantified from variation in 141,456 humans. Nature *581*, 434–443. https://doi.org/10.1038/s41586-020-2308-7.

43. Vaser, R., Adusumalli, S., Leng, S.N., Sikic, M., and Ng, P.C. (2016). SIFT missense predictions for genomes. Nat. Protoc. *11*, 1–9. https://doi.org/10.1038/nprot.2015.123.

44. Adzhubei, I., Jordan, D.M., and Sunyaev, S.R. (2013). Predicting functional effect of human missense mutations using PolyPhen-2. Curr Protoc Hum Genet *Chapter*. Curr. Protoc. Hum. Genet. *Chapter 7*. Unit7 20. https://doi.org/10.1002/0471142905.hg0720s76.

45. Chun, S., and Fay, J.C. (2009). Identification of deleterious mutations within three human genomes. Genome Res. *19*, 1553–1561. https://doi.org/10.1101/gr.092619.109.

46. Schwarz, J.M., Cooper, D.N., Schuelke, M., and Seelow, D. (2014). MutationTaster2: mutation prediction for the deep-sequencing age. Nat. Methods *11*, 361–362. https://doi.org/10.1038/nmeth.2890.

47. Reva, B., Antipin, Y., and Sander, C. (2011). Predicting the functional impact of protein mutations: application to cancer genomics. Nucleic Acids Res. *39*, e118. https://doi.org/10.1093/nar/gkr407.

48. Shihab, H.A., Gough, J., Cooper, D.N., Stenson, P.D., Barker, G.L.A., Edwards, K.J., Day, I.N.M., and Gaunt, T.R. (2013). Predicting the functional, molecular, and phenotypic consequences of amino acid substitutions using hidden Markov models. Hum. Mutat. *34*, 57–65. https://doi.org/10.1002/humu.22225.

49. Kircher, M., Witten, D.M., Jain, P., O'Roak, B.J., Cooper, G.M., and Shendure, J. (2014). A general framework for estimating the relative pathogenicity of human genetic variants. Nat. Genet. *46*, 310–315. https://doi.org/10.1038/ng.2892.

50. Douville, C., Masica, D.L., Stenson, P.D., Cooper, D.N., Gygax, D.M., Kim, R., Ryan, M., and Karchin, R. (2016). Assessing the Pathogenicity of Insertion and Deletion Variants with the Variant Effect Scoring Tool (VEST-Indel). Hum. Mutat. *37*, 28–35. https://doi.org/10.1002/humu.22911.

51. Fleming, S.J., Chaffin, M.D., Arduini, A., Akkad, A.D., Banks, E., Marioni, J.C., Philippakis, A.A., Ellinor, P.T., and Babadi, M. (2023). Unsupervised removal of systematic background noise from droplet-based single-cell experiments using CellBender. Nat. Methods *20*, 1323–1335. https://doi.org/10.1038/s41592-023-01943-7.

52. Germain, P.L., Lun, A., Garcia Meixide, C., Macnair, W., and Robinson, M.D. (2021). Doublet identification in single-cell sequencing data using scDblFinder. F1000Res. *10*, 979. https://doi.org/10.12688/f1000research.73600.2.

53. MacParland, S.A., Liu, J.C., Ma, X.Z., Innes, B.T., Bartczak, A.M., Gage, B.K., Manuel, J., Khuu, N., Echeverri, J., Linares, I., et al. (2018). Single cell RNA sequencing of human liver reveals distinct intrahepatic macrophage populations. Nat. Commun. *9*, 4383. https://doi.org/10.1038/s41467-018-06318-7.

54. Hao, Y., Hao, S., Andersen-Nissen, E., Mauck, W.M., Zheng, S., Butler, A., Lee, M.J., Wilk, A.J., Darby, C., Zager, M., et al. (2021). Integrated analysis of multimodal single-cell data. Cell *184*, 3573–3587.e29. https://doi.org/10.1016/j.cell.2021.04.048.

55. Choudhary, S., and Satija, R. (2022). Comparison and evaluation of statistical error models for scRNA-seq. Genome Biol. *23*, 27. https://doi.org/10.1186/s13059-021-02584-9.

56. Cheng, C., Easton, J., Rosencrance, C., Li, Y., Ju, B., Williams, J., Mulder, H.L., Pang, Y., Chen, W., and Chen, X. (2019). Latent cellular analysis robustly reveals subtle diversity in large-scale single-cell RNA-seq data. Nucleic Acids Res. *47*, e143. https://doi.org/10.1093/nar/gkz826.

57. Ianevski, A., Giri, A.K., and Aittokallio, T. (2022). Fully-automated and ultra-fast cell-type identification using specific marker combinations from single-cell transcriptomic data. Nat. Commun. *13*, 1246. https://doi.org/10.1038/s41467-022-28803-w.

58. Finak, G., McDavid, A., Yajima, M., Deng, J., Gersuk, V., Shalek, A.K., Slichter, C.K., Miller, H.W., McElrath, M.J., Prlic, M., et al. (2015). MAST: a flexible statistical framework for assessing transcriptional changes and characterizing heterogeneity in single-cell RNA sequencing data. Genome Biol. *16*, 278. https://doi.org/10.1186/s13059-015-0844-5.

59. Gennady Korotkevich, V.S., Budin, N., Shpak, B., Artyomov, M.N., and Sergushichev, A. (2021). Fast gene set enrichment analysis. Preprint at bioRxiv. https://doi.org/10.1101/060012.

60. Vasaikar, S.V., Deshmukh, A.P., den Hollander, P., Addanki, S., Kuburich, N.A., Kudaravalli, S., Joseph, R., Chang, J.T., Soundararajan, R., and Mani, S.A. (2021). EMTome: a resource for pan-cancer analysis of epithelial-mesenchymal transition genes and signatures. Br. J. Cancer *124*, 259–269. https://doi.org/10.1038/s41416-020-01178-9.

61. Fumarola, C., La Monica, S., Alfieri, R.R., Borra, E., and Guidotti, G.G. (2005). Cell size reduction induced by inhibition of the mTOR/S6K-signaling pathway protects Jurkat cells from apoptosis. Cell Death Differ. *12*, 1344–1357. https://doi.org/10.1038/sj.cdd.4401660.

62. La Monica, S., Galetti, M., Alfieri, R.R., Cavazzoni, A., Ardizzoni, A., Tiseo, M., Capelletti, M., Goldoni, M., Tagliaferri, S., Mutti, A., et al. (2009). Everolimus restores gefitinib sensitivity in resistant non-small cell lung cancer cell lines. Biochem. Pharmacol. *78*, 460–468. https://doi.org/10.1016/j.bcp.2009.04.033.

63. Cavazzoni, A., Alfieri, R.R., Carmi, C., Zuliani, V., Galetti, M., Fumarola, C., Frazzi, R., Bonelli, M., Bordi, F., Lodola, A., et al. (2008). Dual mechanisms of action of the 5-benzylidene-hydantoin UPR1024 on lung cancer cell lines. Mol. Cancer Ther. *7*, 361–370. https://doi.org/10.1158/1535-7163.MCT-07-0477.